AD-A155 622 EXPERIMENTAL AND THEORETICAL ASSESSMENT OF A NEW TECHNIQUE FOR TH NON-DE.. (U) OHIO STATE UNIV RESEARCH FOUNDATION COLUMBUS V H KENNER 21 FEB 85 1/1

UNCLASSIFIED AFWAL-TR-84-4129 F33615-82-K-5009 F/G 11/4 NL

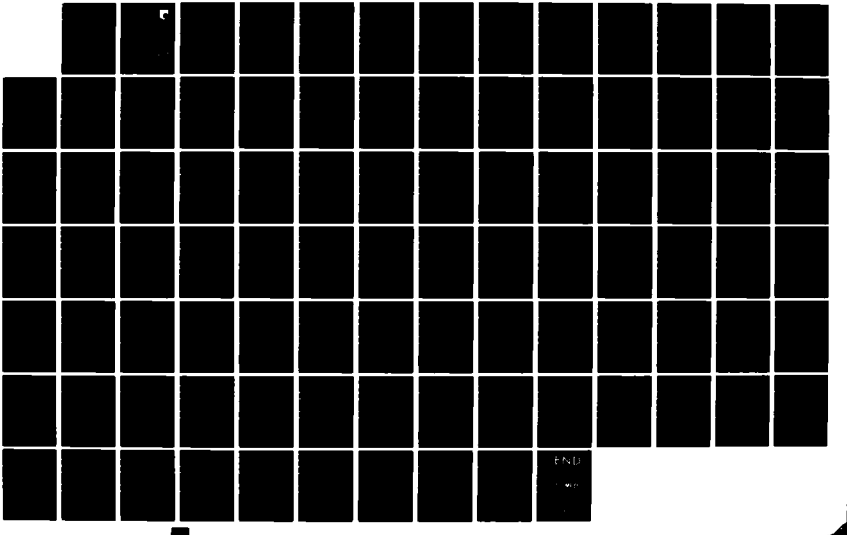

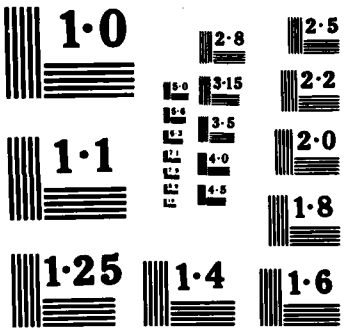

AFWAL-TR-84-4129

V. H. KENNER

OHIO STATE UNIVERSITY RESEARCH FOUNDATION
COLUMBUS, OH 43212

EXPERIMENTAL AND THEORETICAL ASSESSMENT OF A NEW TECHNIQUE FOR THE NON-DESTRUCTIVE EVALUATION OF LAMINATED PANELS

February 21, 1985

Final Report for Period February 1982 - June 1984

MATERIALS LABORATORY
AIR FORCE WRIGHT AERONAUTICAL LABORATORIES
AIR FORCE SYSTEMS COMMAND
WRIGHT PATTERSON AIR FORCE BASE, OHIO 45433

NOTICE

When Government drawings, specifications, or other data are used for any purpose other than in connection with a definitely related Government procurement operation, the United States Government thereby incurs no responsibility nor any obligation whatsoever; and the fact that the government may have formulated, furnished, or in any way supplied the said drawings, specifications, or other data, is not to be regarded by implication or otherwise as in any manner licensing the holder or any other person or corporation, or conveying any rights or permission to manufacture use, or sell any patented invention that may in any way be related thereto.

This report has been reviewed by the Office of Public Affairs (ASD/PA) and is releasable to the National Technical Information Service (NTIS). At NTIS, it will be available to the general public, including foreign nations.

This technical report has been reviewed and is approved for publication.

ROBERT L. CRANE
Nondestructive Evaluation Branch
Metals and Ceramics Division

FOR THE COMMANDER

D. M. FORNEY, JR., Chief
Nondestructive Evaluation Branch
Metals and Ceramics Divison

"If your address has changed, if you wish to be removed from our mailing list, or if the addressee is no longer employed by your organization please notify AFWAL/MLLP, *W-PAFB, OH 45433 to help us maintain a current mailing list".*

Copies of this report should not be returned unless return is required by security considerations, contractual obligations, or notice on a specific document.

6c. ADDRESS (City, State and ZIP Code)		7b. ADDRESS (City, State and ZIP Code)
1314 Kinnear Rd. Columbus, OH 43212		Wright Patterson AFB, OH 45433
8a. NAME OF FUNDING/SPONSORING ORGANIZATION	8b. OFFICE SYMBOL (If applicable)	9. PROCUREMENT INSTRUMENT IDENTIFICATION NUMBER F33615-82-K-5009
8c. ADDRESS (City, State and ZIP Code)		10. SOURCE OF FUNDING NOS.

PROGRAM ELEMENT NO.	PROJECT NO.	TASK NO.	WORK UNIT NO.
610100	ILIR	01	45

11. TITLE (Include Security Classification) Experimental and Theoretical Assessment of a New Technique for the Non-Destructive Evaluation of Laminated Panels

12. PERSONAL AUTHOR(S) V. H. Kenner

13a. TYPE OF REPORT	13b. TIME COVERED	14. DATE OF REPORT (Yr., Mo., Day)	15. PAGE COUNT
Final Report	FROM 18Feb82 TO 30Jun84	February 21, 1985	

16. SUPPLEMENTARY NOTATION

17. COSATI CODES			18. SUBJECT TERMS (Continue on reverse if necessary and identify by block number)
FIELD	GROUP	SUB. GR.	
20	01		Adhesive bond quality control; laminated panel quality control; plate waves.
11	04		

19. ABSTRACT (Continue on reverse if necessary and identify by block number)

A theoretical and experimental analysis of the low frequency vibration response of bonded joints showed that it is possible to distinguish between mechanically sound and debonded specimans using a low frequency analysis. This analysis has shown that it is indeed possible to construct a field-usable instrument that would permit rapid inspection of bonded structures for degrading conditions that occur at the edges of bonded joints. This analysis is applicable to both composite and metal laminated structures.

20. DISTRIBUTION/AVAILABILITY OF ABSTRACT	21. ABSTRACT SECURITY CLASSIFICATION
UNCLASSIFIED/UNLIMITED ☒ SAME AS RPT. ☐ DTIC USERS ☐	Unclassified

22a. NAME OF RESPONSIBLE INDIVIDUAL	22b. TELEPHONE NUMBER (Include Area Code)	22c. OFFICE SYMBOL
Robert L. Crane	513/255-5561	AFWAL/MLLP

TABLE OF CONTENTS

TABLE OF CONTENTS
(continued)

LIST OF ILLUSTRATIONS

LIST OF TABLES

1. INTRODUCTION

1.1 Goal

The goal of the present research project was to evaluate a potential method of edge flaw detection in laminated structures. This method utilizes miniature dynamic force transducers to detect the changes in loading history arising from the (very low level) impact of steel spheres on the transducer, which is located on the surface of the examined object. Both adhesively bonded laminates and laminated composite materials were examined.

1.2 Background

The detection of defects in laminated structural members has attracted considerable attention in recent years. This is due both to the potential advantages that such construction offers in weight savings, ease of fabrication and fatigue life and also to the relatively greater uncertainty in predicting service life for these comparatively new types of structures. A variety of possible techniques has been considered previously, and review articles describing such methods are available[1.1-1.3].

In the present study the emphasis is on a method of flaw detection oriented toward in-service inspection as opposed to quality control associated with initial manufacture. Accordingly the emphasis is on detection of flaws near edges of adhesively joined members because it is primarily at these boundaries where flaws associated

with service occur. This is so because, typically, stresses are greatest at the boundary and because degradation owing to contamination by, e.g., moisture absorption, initiates on the perimeter. The locality of flaws developed in-service thus mitigates against the use of ultrasonic inspection methods which suffer from difficulties such as edge dispersion in the vicinity of boundaries.

The method of flaw detection described in this report, in some aspects, represents a quantification of the familiar "tapping" or "coin tap" test in which a light tap by a coin or other standardized striker is used to qualitatively differentiate between bonded and unbonded structure by a change in frequency of the emanated sound [1.1-1.3]. In our method the effect of a debond on the force history experienced by a small dynamic load transducer interposed between the structure of interest and a spherical striker travelling at very low velocity is observed. Thus, the present method can take advantage of structure-induced changes in the loading history itself rather than only detecting changes in the subsequent "ringing," as is done in the traditional tapping inspection. The advantage of the present technique is in providing a quantifiable signal, several features of which provide, at least potentially, indicators of structural integrity for laminated structures. We note here that the emphasis of the present investigation is on understanding the physical basis for a possible nondestructive evaluation technique. Thus, while the drop test utilized to produce low-velocity impulsive loading suits our purpose well, it

is likely not the optimal method for producing such loads from the point of view of designing a high efficiency inspection procedure.

1.3 Summary of Accomplishments

Target plates which were fabricated by bonding two 0.080-inch-thick aluminum plates with FM-73M adhesive and which contained semi-circular artificial edge flaws ranging from 1/8-inch to 2-inches in radius have been examined using low-level impact loading. Similar targets fabricated from fiberglass-epoxy and graphite-epoxy prepreg tapes have also been examined. Several variations of the piezoelectric transducer have been utilized in these tests. A test configuration in which the target plate is struck at a site remote from the transducer was also explored. Spectral analysis of the transducer output has been carried out for many of the cases tested. A modelling effort using the finite element method has been pursued in order to better understand the basic phenomena underpinning the technique and to eventually provide a predictive tool. Finally, strain gages have been attached on one of the aluminum targets in order to provide more complete data for correlation with the model.

1.4 Conclusions

Several conclusions have been derived from the test results as follows:

- Several features of the transducer output are capable of indicating the presence of flaws. Among these are the peak amplitude,

the shape and the frequency domain representation (Fourier Transform) of the pulse.

- A significant portion of the information derivable from the experimental records is contained in the ringing part of the history which occurs subsequent to impact. In view of this observation a series of "remote" tests was conducted in which the target was loaded by impact at a site remote from the transducer. This technique accentuates the difference between on-debond and off-debond responses.

- Flaw detection becomes increasingly difficult as the flaw plan dimension approaches plate thickness. For example, for two 0.080-inch-thick bonded aluminum plates, a flaw of ¼-inch radius represented the limits of detectibility in the present analysis.

- Strain gages applied to the bottom surface of a top-loaded flaw show that the relationship between loading and response is significantly nonlinear in nature. Modelling of this dynamic contact proves difficult.

1.5 Format of Report Details

The experimental apparatus is described in Section 2. Sections 3 and 4 represent the status of the investigation as prepared for presentation during its course. In Section 3 some results from the fiberglass-epoxy target, B3, and from the first two bonded aluminum

plates (A1 and A2) are presented, while Section 4 discusses the bulk of results from graphite-epoxy targets C1, C2, C3. Section 5 details some experiments conducted more recently. Section 6 discusses the finite element modelling effort.

1.6 References

1.1. Hagemaier, D.J., "Bonded joints and non-destructive testing 1. Bonded honeycomb structures," Non-destructive Testing, v. 4, pp. 401-407, December 1971.

1.2. Schliekelmann, R.J., "Non destructive testing of adhesive bonded metal-to-metal joints 1, "Non-destructive Testing, v. 5, pp. 79-86, April 1972.

1.3. Schliekelmann, R.J., "Non-destructive testing of adhesive bonded metal-to-metal joints 2," Non-destructive Testing, v. 5, pp. 144-154, June 1972.

2. EXPERIMENT

2.1 Targets

Plate targets utilizing three different materials - bonded aluminum, fiberglass-epoxy composite and graphite-epoxy composite have been fabricated and tested. All have contained artificial flaws consisting of Kapton film to produce a debonded region of semicircular shape with the diametral boundary coincident with the plate edge, as shown in Fig. 3.2. A summary of the tragets fabricated is given in Table 2.1. In targets fabricated early in the program a single flaw was centered on a plate long edge; later, an aluminum target, A4, contained two flaws per long edge.

The bonded aluminum plates were made from 2024-T4 sheet stock bonded with a single layer of FM-73M adhesive film supplied by American Cyanamid Company, Harve de Grace, Maryland. This bonding agent, which includes skrim cloth, is obtained in a roll and the adhesive layer is initially approximately 0.005-inches-thick. Debonds in these targets were simulated by inserting a single layer of 0.0004-inch-thick Kapton film between the adhesive layer and one of the plates. The final bond thickness was nominally 0.004 inches. In one specimen, A3, a thicker bond was generated by using two FM-73M layers; in this instance the defect was generated by removing a semi-circular piece of the adhesive layer. In early targets, the adhesive was cured by compressing the target between ½-inch-thick teflon-coated steel plates which were clamped by bolts. The combination of

TABLE 2.1

Summary of Targets

Identification	Plan Dimensions	Thickness	Flaw Radii
Series A - Bonded Aluminum			
A1	10x20	.165	1
A2	10x20	.163	½, 2
A3	10 1/8x15 3/4	.169	½, 1
A4	10x20	.163	1/8,¼,½,1
Series B - Fiberglass-Epoxy			
B1	17¼x8	.120	1
B2	17 3/8x8	.116	1"
B3	17 3/8 x 8	.120	½, 2
B4	17 3/8, 8	.117	½, 1
Series C - Graphite-Epoxy (AS4/3502)			
C1	17 3/4x7 5/8	.108	½, 1
C2	17 3/4x7 5/8	.113	2
C3	12x5 3/4	.121	¼, ½

spring-washers under the clamping bolts and torque-wrench controlled tightening was found to yield satisfactory results. Heating was accomplished by placing this assembly in an oven. The acquisition of a hot press later in the program simplified the process of target fabrication but did not significantly change the quality of the bonded plates.

The fiberglass-epoxy panels were composed of twelve layers of preimpregnatd tape to generate unidirectional fibers oriented parallel to the long side of these panels. The clamping fixture described above was again utilized to provide the required surface pressure. Debonds were generated at mid-thickness by interposing two semicircular pieces of Kapton film between plies in targets B1, B2, and B3; in B4 the flaws were located at a depth of ¼ of the thickness.

The graphite-epoxy targets were fabricated from an AS4/3502 system supplied by Hercules Corporation of Magna, Utah, in the form of a 6-inch-wide preimpregnated tape. These panels consisted of twenty alternating $0^{\circ}/90^{\circ}$ plies which were symmetric about the mid-plane. The flaws again were generated by placing two semicircular layers of Kapton between the middle plies. No bleeding of the resin was provided for so that these panels were epoxy rich. After curing, the edges of the panels were milled to yield the final target.

2.2 Transducers

The transducers used in this investigation are substantially identical in configuration to the miniature force transducers described in Reference 2.1. These devices use two piezoelectric X-cut quartz crystals as the active elements. Previous evaluation of them indicated that these load sensors were capable of measuring loads, generated by low-velocity impact (on the transducers) of small steel spheres, of approximately 20 microseconds in duration with an accuracy in the neighborhood of 5 percent. The use of two crystals was necessitated by the need to eliminate the contribuions of certain bending deformations from the transducer output. In the present case both the quartz crystals and the brass disks are 0.050-inch-thick. A replaceable steel disk of the same thickness is wrung to the top of the transducer with a small amount of grease and provides the actual surface upon which the steel striker impinges. Three transducers of this type have been utilized to date. The first two differ only in diameter - 0.50 and 0.25-inches, respectively, while the third utilized thinner, 0.020-inch-thick, brass disks and was fabricated in order to evaluate the effect of this design variable on transducer outpout.

A fourth transducer was constructed in which only a single crystal was used. This sensor had a diameter of 1/8 inch and the X-cut quartz crystal, 0.050-inch-thick, was sandwiched between two disks of hardened steel drill rod which were 0.023-inches-thick. This transducer

represents the smallest such device that we could fabricate "by hand" and was used to see if a smaller transducer provided increased resolution for detecting small debonds.

While the transducers described above originated as force transducers, it became clear during the course of the experiments that, after impact was completed, the transducer continued to provide useful information in the ringing portion of the record. As discussed in greater detail in the sequel, this response is associated with acceleration of the transducer. Since this acceleration outpout of the transducer is small compared to the outpout generated directly by contact forces between the transducer and the striker during impact, a number of tests were conducted in which the target was struck at a position remote from the transducer. When utilized for these remote tests, additional mass was sometimes added to the top of the transducer in the form of a metal cylinder affixed by wringing with a small amount of grease or by bonding with cyanoacrylic adhesive.

2.3 Test Configuration

The flawed panels were clamped, at the edge opposite that containing the flaw, to an x-y stage which permitted positioning to within 0.001 inch. Steel spheres of 0.5-inch diameter were dropped a distance of 12 inches in initial tests. Later this distance was reduced to approximately 2 inches. The 0.125-inch diameter steel strikers dropped a distance of 3.31 inches from a drop fixture which held the striker until release. Initially, the drop fixture utilized

a switched electromagnet, but it was found that a fixture which utilized orally applied suction to hold the striker provided both better drop accuracy and less difficulty with premature triggering of the oscilloscope used to record transducer output. The drop fixture was in turn supported by a dial indicator stand which was magnetically affixed to a massive steel surface. The x-y stage was bolted to this surface as well. A miniature plumb bob was constructed to hang from the drop fixture for close location of the impact site.

The above efforts notwithstanding, it was found that to assure the best repeatability from run-to-run with the smallest strikers additional precautions were necessary. First, it was found that both steel and aluminum protector disks were minutely dented by the hardened steel strikers, even at the low impact velocities employed. This produced some randomness in the test results which we attributed to variations in the impact surface properties due to localized work hardening associated with prior impacts. Thus, the protector disks ultimately employed were machined from drill rod, hardened and then ground. Second, it was found that very small amounts (i.e., only indirectly detectible) of grease and oil present on either the 0.125-inch-diameter strikers or the protector disk surface could substantially affect the force-time history. A procedure in which the spheres were washed in acetone, only dropped once before re-washing, and never touched by hand after washing and prior to dropping satisfactorily eliminated this problem.

2.4 Transducer Circuit

A capacitor was placed in parallel with the double crystal transducer to suitably extend the long-time frequency response of the circuit; the total circuit capacitance was measured with an impedence bridge and found to be 2.07 nF. The crystal output was fed directly into a digital oscilloscope which recorded two points per microsecond for a minimum duration of 512 microseconds. This record was than stored on a 5¼-inch floppy diskette contained in a disk drive integral to the oscilloscope main frame.

2.5 Strain Gages

In order to better observe the plate response for loading over, as opposed to away from a debond, strain gages were affixed to the underside of target A4. Owing to the extremely low strain levels encountered - of the order of 1×10^{-6}, semiconductor gages were required to provide suitable output. The gages were connected in a potentiometer circuit with 15 VDC excitation voltage; gage outpouts were capacitively coupled to the digital oscilloscope.

2.6 References

2.1. Kenner, V.H., "On the Use of Quartz Crystals in Dynamic Stress and Force Transducers," Experimental Mechanics, V. 15, pp. 102-106, 1975.

3. A STUDY OF FLAW IDENTIFICATION IN ADHESIVE BONDS USING A TECHNIQUE OF IMPACT MODIFICATION

V. H. KENNER, G. H. STAAB AND H.-S. JING

Department of Engineering Mechanics
The Ohio State University
Columbus, Ohio

3.1 Abstract

A small load transducer has been used to obtain force histories arising from the impact of steel spheres with flawed, laminated plates. The modification of the force-time record in the presence of the flaw is used for the detection of same. Tests are reported for both bonded aluminum and glass-epoxy composite plates.

3.2 Introduction

The detection of defects in laminated structural members has attracted considerable attention in recent years. This is due both to the potential advantages that such construction offers in weight savings, ease of fabrication and fatigue life and also to the relatively greater uncertainty in predicting service life for these comparatively new types of structures. A variety of possible techniques have been considered previously, and review articles describing such methods are available[3.1-3.3].

In the present study the emphasis is on a method of flaw detection oriented toward in-service inspection as opposed to quality control associated with initial manufacture. Accordingly, the emphasis is on detection of flaws near edges of adhesively joined members because it is primarily at these boundaries where flaws associated with service occur. This is so because, typically, stresses are greatest at the boundary and because it is on the perimeter that degradation due to bond contamination, by, e.g., moisture absorption, initiates.

The method of flaw detection described in this paper, in some aspects, represents a quantification of the familiar "tapping" or "coin tap" test in which a light tap by a coin or other standardized striker is used to qualitatively differentiate between bonded and unbonded structure by a change in frequency of the emanated sound[3.1-3.3]. In our method the effect of a debond on the force history experienced by a small dynamic load transducer interposed

between the structure of interest and a spherical striker travelling at very low velocity is observed. Thus, the present method can take advantage of structure-induced changes in the loading history itself rather than only detecting changes in the subsequent "ringing," as is done in the traditional tapping inspection. The advantage of the present technique is in providing a quantifiable signal, several features of which provide, at least potentially, indicators of structural integrity for laminated structures. We note here that the emphasis of the present investigation is on understanding the physical basis for a possible non-destructive evaluation technique. Thus, while the drop test utilized to produce low-velocity impulsive loading suits our purposes well, it is likely not the optimal method for producing such loads from the point of view of designing a high efficiency inspection procedure.

3.3 Experiment

The miniature force transducers used in this investigation are substantially identical in configuration to those described in Reference (3.4), and are depicted schematically in Fig. 3.1. These transducers use two piezoelectric X-cut quartz crystals as the active elements. Previous evaluation of them[3.4] indicated that these load sensors were capable of measuring loads, generated by low-velocity impact (on the transducers) of small steel spheres, of approximately 20 microseconds in duration with an accuracy in the

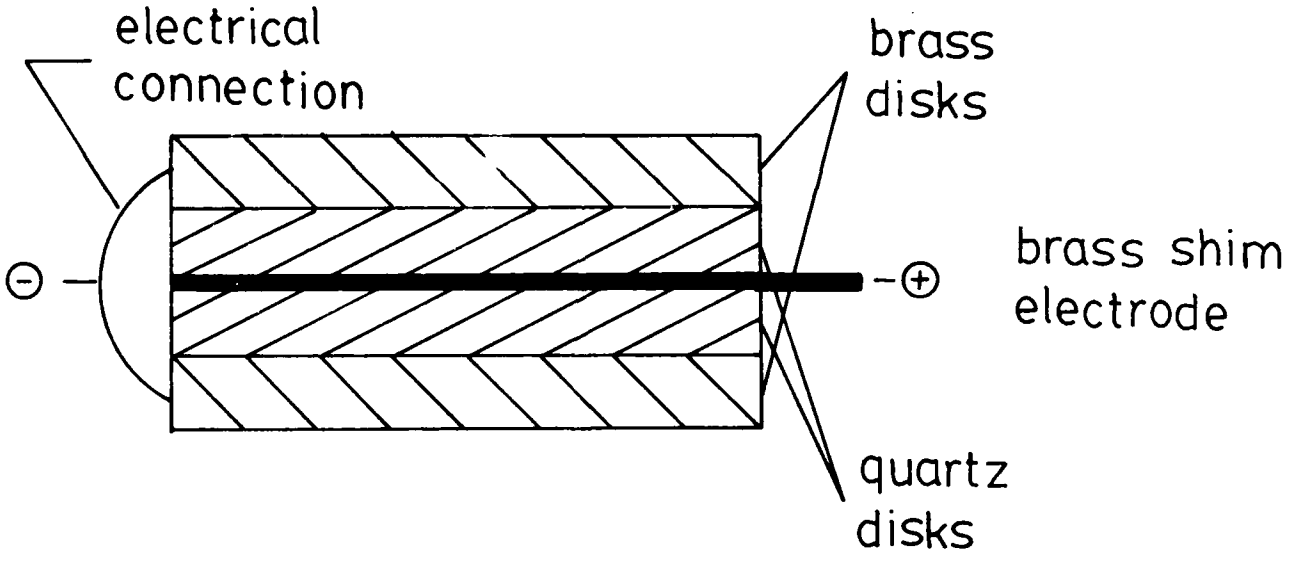

3.1. Schematic cross-section of the miniature load transducer.

neighborhood of 5%. The use of two crystals was necessitated by the need to eliminate the contributions of certain bending deformations from the transducer output. In the present case both the quartz crystals and the brass disks are 0.050-inch (1.27-mm)-thick while the brass shim electrode was 0.020-inch (0.50 mm)-thick. A replaceable steel disk of the same thickness is wrung to the top of the transducer with a small amount of grease and provides the actual surface upon which the steel striker impinges. Three transducers of this type have been utilized to date. The first two differ only in diameter -- 0.50 and 0.25-inches (12.7 and 6.35-mm), respectively, while the third utilized thinner, 0.020-inch (0.51-mm)-thick, brass disks and was fabricated in order to evaluate the effect of this design variable on transducer output.

Two plate types have been tested. The first type consists of two 2040-T4 aluminum plates, each 10 x 20 x 0.080 inches (254 x 508 x 2.03-mm) bonded together with FM-73M (American Cyanamid, Havre de Grace, Maryland) structural adhesive. This bonding agent, which includes skrim cloth, is obtained in a roll, and the adhesive layer is approximately 0.005-inches (0.13-mm)-thick. Debonds were simulated by inserting a single layer of polymeric film (Kapton) which was approximately 0.0004-inches (0.010-mm)-thick between the adhesive layer and one of the plates. The final bond thickness, after curing at elevated temperature with clamping pressure according to the manufacturer's instructions, was 0.003-inch (0.076-mm). The

debonds tested were semicircular with radii of 1/2, 1 and 2-inches (12.7, 25.4 and 50.8-mm), respectively. The center of curvature for the debond semicircle was always located at the plate edge and midway along the long side of the plate.

The second configuration consisted of a 17 x 8 x 0.112-inches (432 x 203 x 2.8-mm) plate fabricated from twelve layers of fiberglass-epoxy "prepreg" with unidirectional fibers oriented parallel to the long side of the plate. A 2-inch (50.8-mm)-radius semicircular defect consisting of two layers of Kapton located at mid-thickness midway along the long side of the plate was examined.

Tests on additional, smaller, specimens of aluminum were conducted in which debonds were generated as described above with the specimens subsequently being sacrificed by machining away one layer of aluminum to expose the debond as well as the adjacent bonded area. It was found that the bonded area contained no visible voids and that the debond was defined to within better than 1/32-inch (0.8-mm).

These targets were supported and tested as depicted in Fig. 3.2. Steel spheres with diameters of 0.5, 0.25 and 0.125-inches (12.7, 6.35 and 3.18-mm), respectively, were first held by a small electro- magnet and then released to fall from drop heights always less than 12-inches (305-mm) onto the force transducer, which was held in place on the target plate by a film of all-purpose grease. With only the addition of an approximately

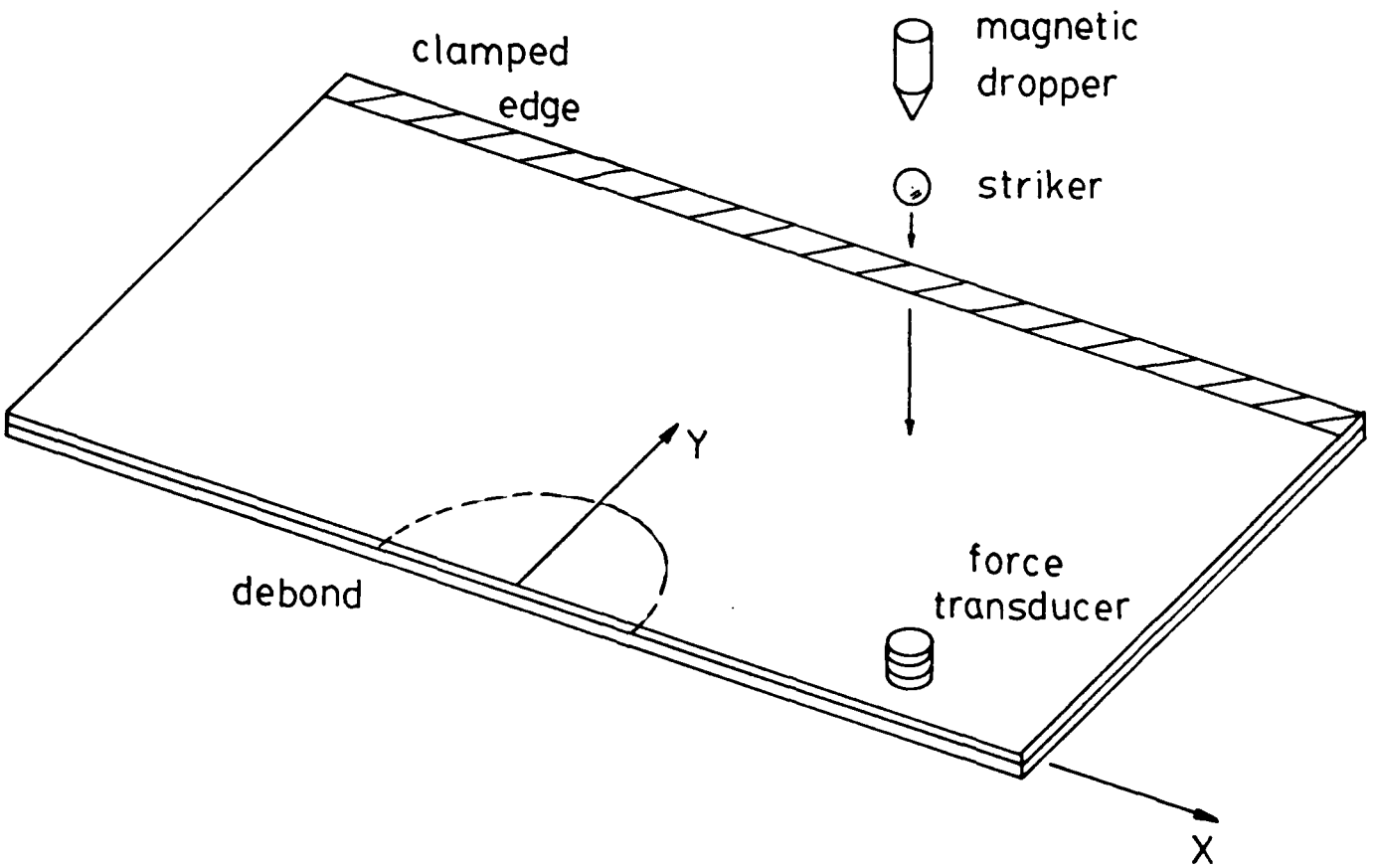

3.2. Test configuration and coordinate system defining impact location (used in subsequent figures).

2000 pf capacitor connected in parallel to provide suitable long-time frequency response, the output of the force transducer was fed into a digital oscilloscope which recorded two points per microsecond. The total circuit capacitance was measured to $\pm$ 10 pf with an impedance bridge. This record of, essentially, force vs. time was then stored on a 5-inch floppy diskette contained in a disk drive integral to the oscilloscope main frame. In turn these data were transferred to an 8-inch floppy disk for subsequent manipulation in our laboratory computer system.

3.4 Results

Experimental results for the 1-inch (25.4-mm) radius flaw in the aluminum target are presented in Figs. 3.3 to 3.5 for selected positions subjected to loading by the 1/2, 1/4 and 1/8-inch (12.75, 6.35 and 3.18-mm) strikers, respectively. In these figures the position is defined by the coordinate system shown in Fig. 3.2, with the flaw centered at the origin. The time-dependent electrical output voltage V(t) of the transducer has been interpreted as proportional to the force F(t) through the relationship[3.4]

$$F(t) = \frac{CV(t)}{2K}$$

where C is the circuit capacitance, and k is the appropriate piezoelectric constant (2.3×10^{12} coulombs/newton).

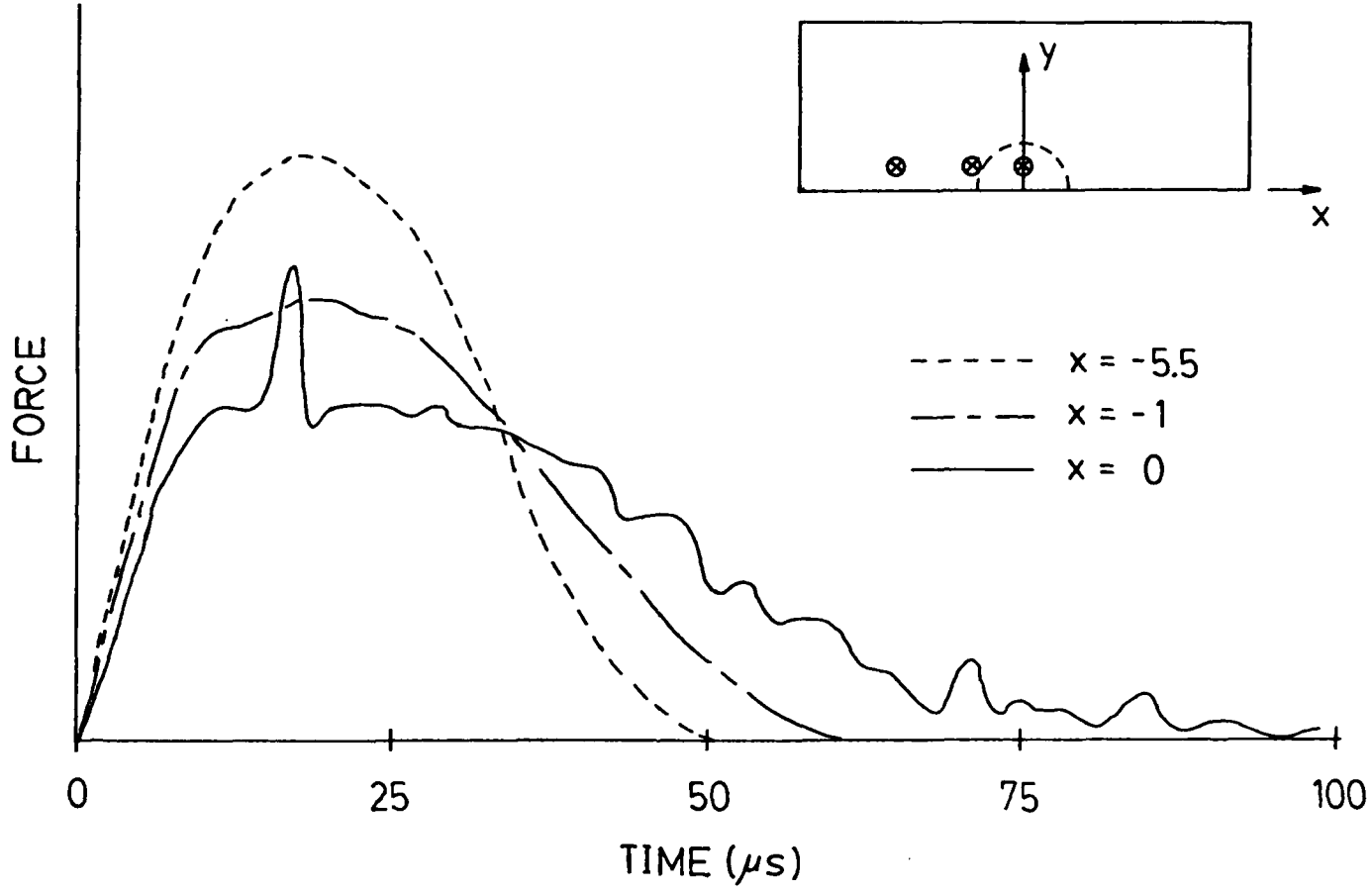

3.3. Loading histories from bonded aluminum plate, 1-inch-radius debond, 1/2-inch-diameter striker, y = 0.5-inch.

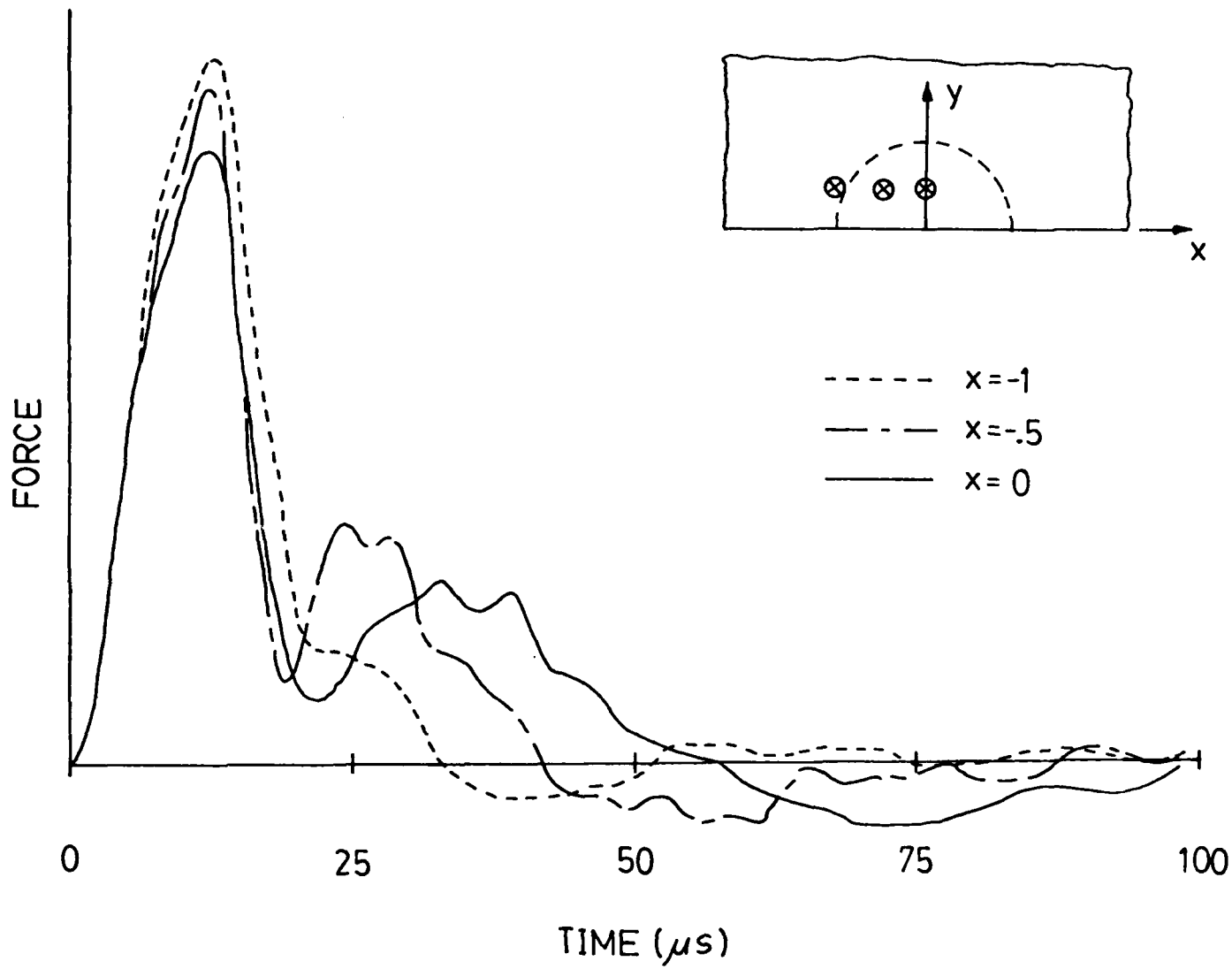

3.4. Loading histories from bonded aluminum plate, 1-inch-radius debond, 1/4-inch-diameter striker y = 0.5 inch.

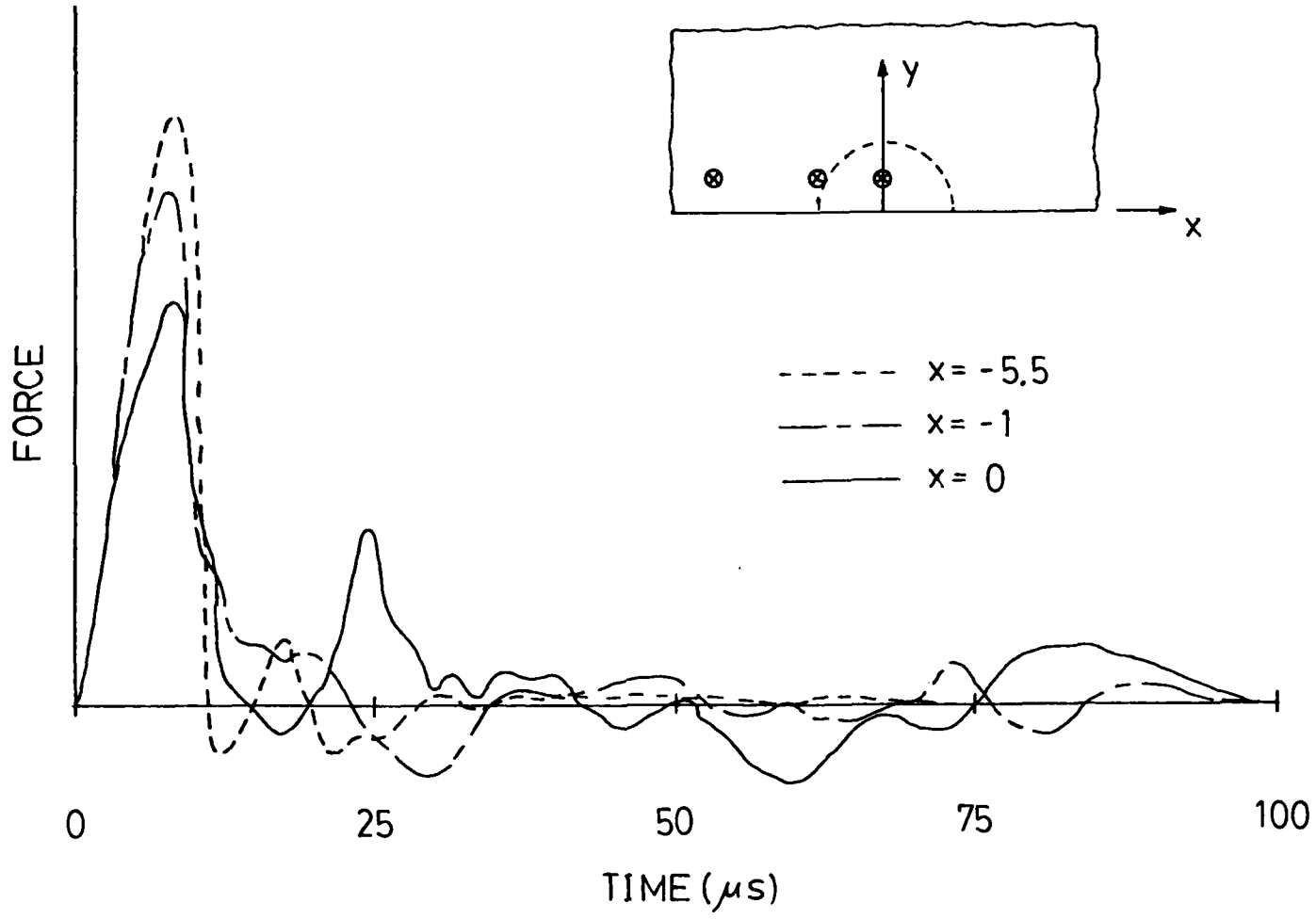

3.5. Loading histories from bonded aluminum plate, 1-inch-radius debond, 1/8-inch-diameter striker, y = 0.5-inch.

The force-time history for the 1/2-inch (12.7-mm)-radius flaw between aluminum plates under impact of a 1/8-inch (3.18-mm) striker is shown in Fig. 3.6. The force histories obtained from a glass-epoxy plate with a 2-inch (50.8-mm) radius flaw using 1/2-inch (12.75-mm) and 1/8-inch (3.18-mm) strikers are shown in Figs. 3.7 and 3.8, respectively.

For the case of the 1-inch (25.4-mm) radius flaw between aluminum plates the frequency spectra for the loading pulses have been obtained through the use of a digital spectrum analyzer (Nicolet Scientific Corp., model 446B). Spectra corresponding to the use of 1/2, 1/4 and 1/8-inch (12.75, 6.35 and 3.18-mm) strikers are presented in Fig. 3.9 for impact away from the flaw, and in Fig. 3.10 for impact over the flaw.

3.5 Discussion and Conclusions

In the present application the miniature force transducers performed at approximately the same accuracy levels as had been reported for them previously.[3.4] This was ascertained on the basis of several comparisons of impulse, calculated from the force-time records, against the change in striker momentum, ascertained from the known initial drop height and the (observed and recorded) rebound height. The piezoelectric constant for the quartz crystals was taken[3.4] to be 10.22×10^{12} coulombs/lb. (2.30×10^{12} coulombs/newton). For a check of two runs on the aluminum target, the impulse averaged 9.8% lower than the measured change in

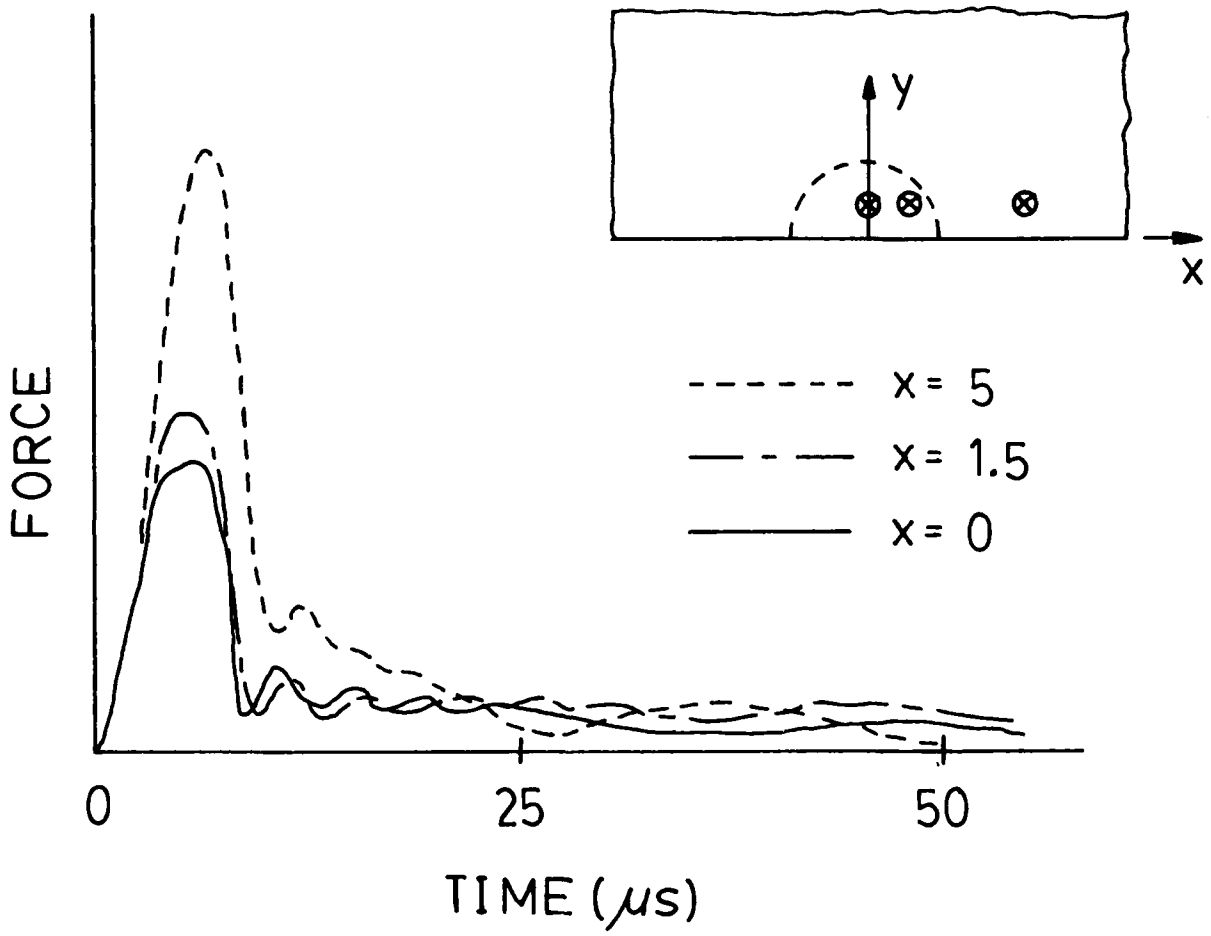

3.6. Loading histories from bonded aluminum plate, 1/2-inch-radius debond, 1/8-inch-diameter striker, y = 0.5-inch.

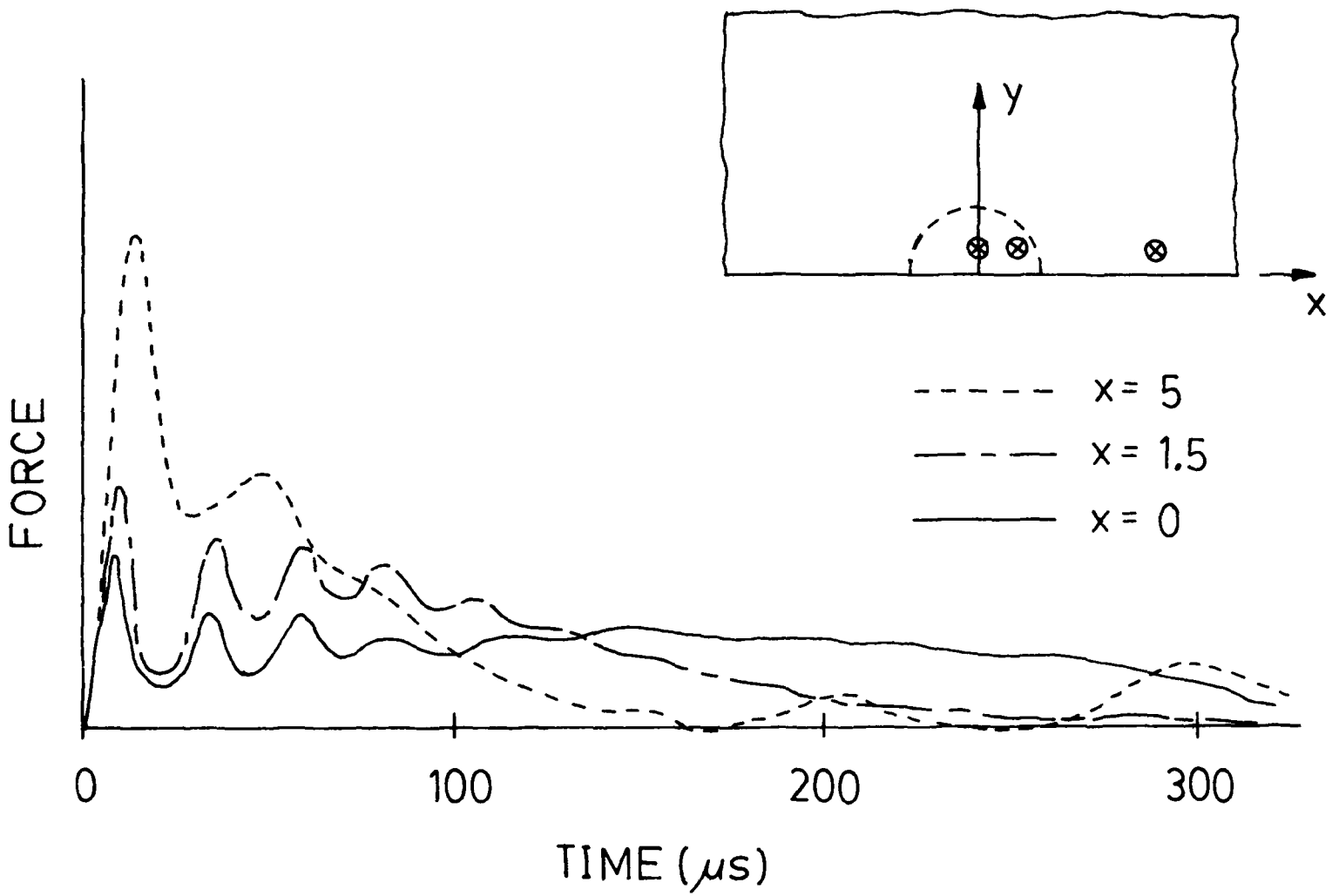

3.7. Loading histories from fiberglass-epoxy plate, 2-inch-radius debond, 1/2-inch-diameter striker, y = 0.5-inch.

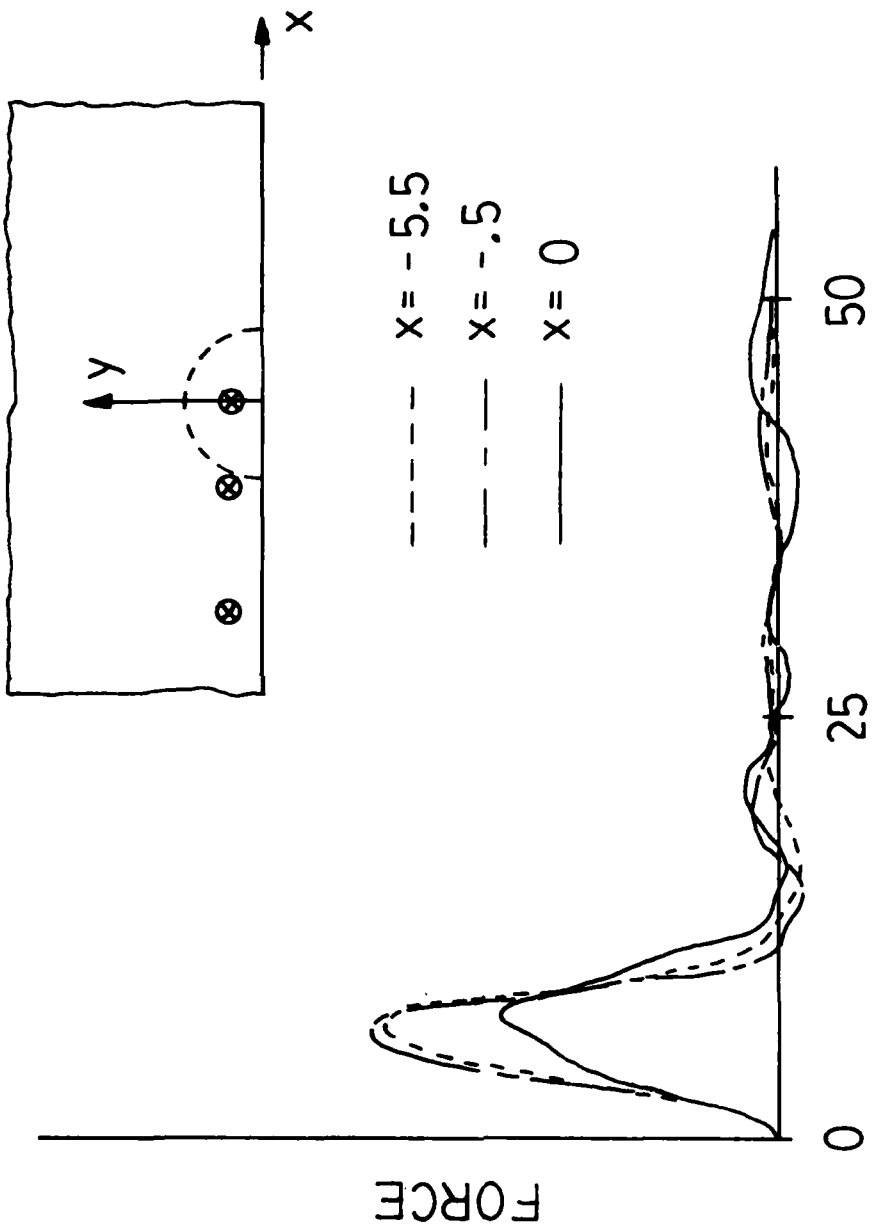

3.8. Loading histories from fiberglass-epoxy plate, 2-inch-radius debond, 1/8-inch-diameter striker, y = 0.5-inch.

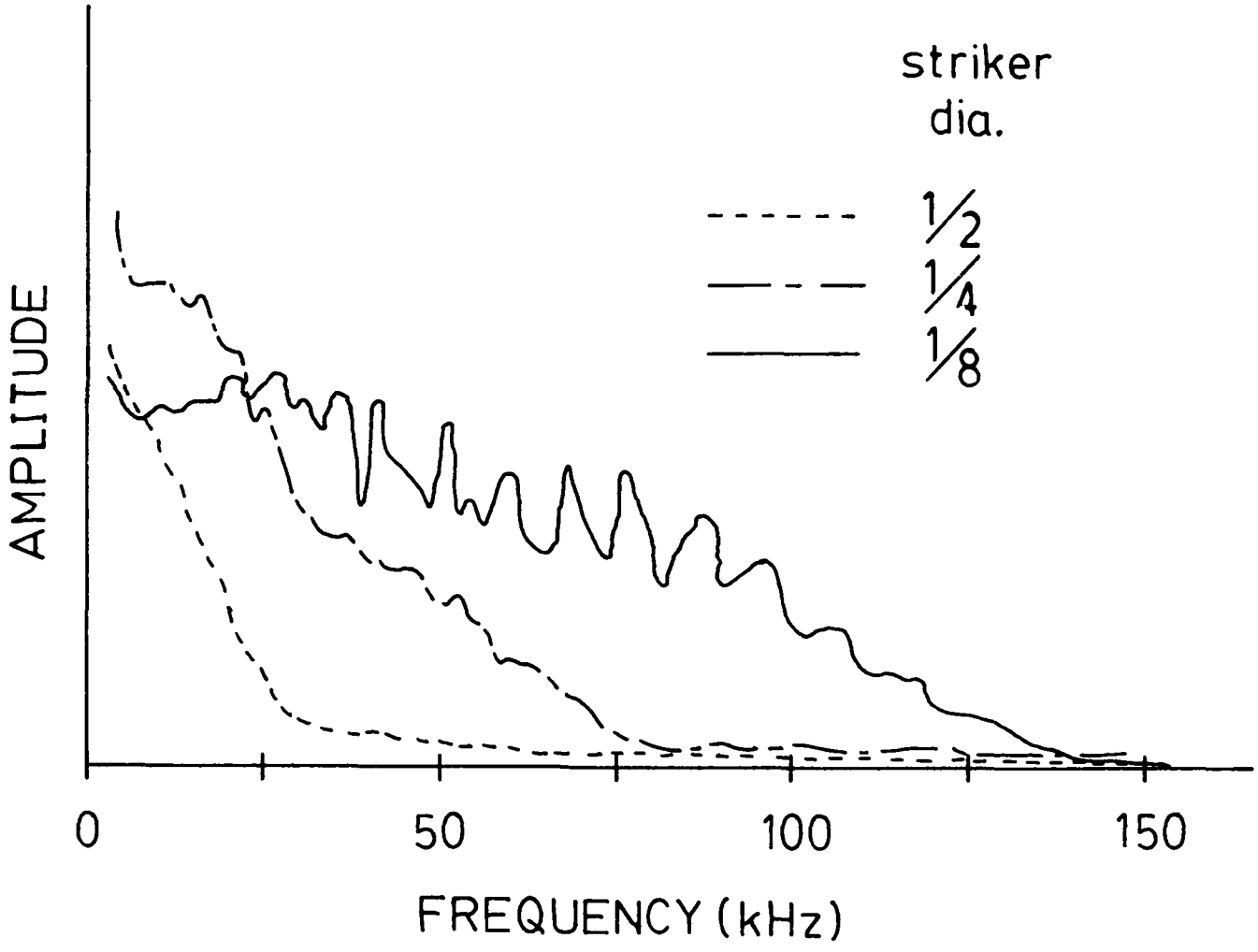

3.9. Frequency domain representation of loading histories away from debond Figures 3.3 to 3.5.

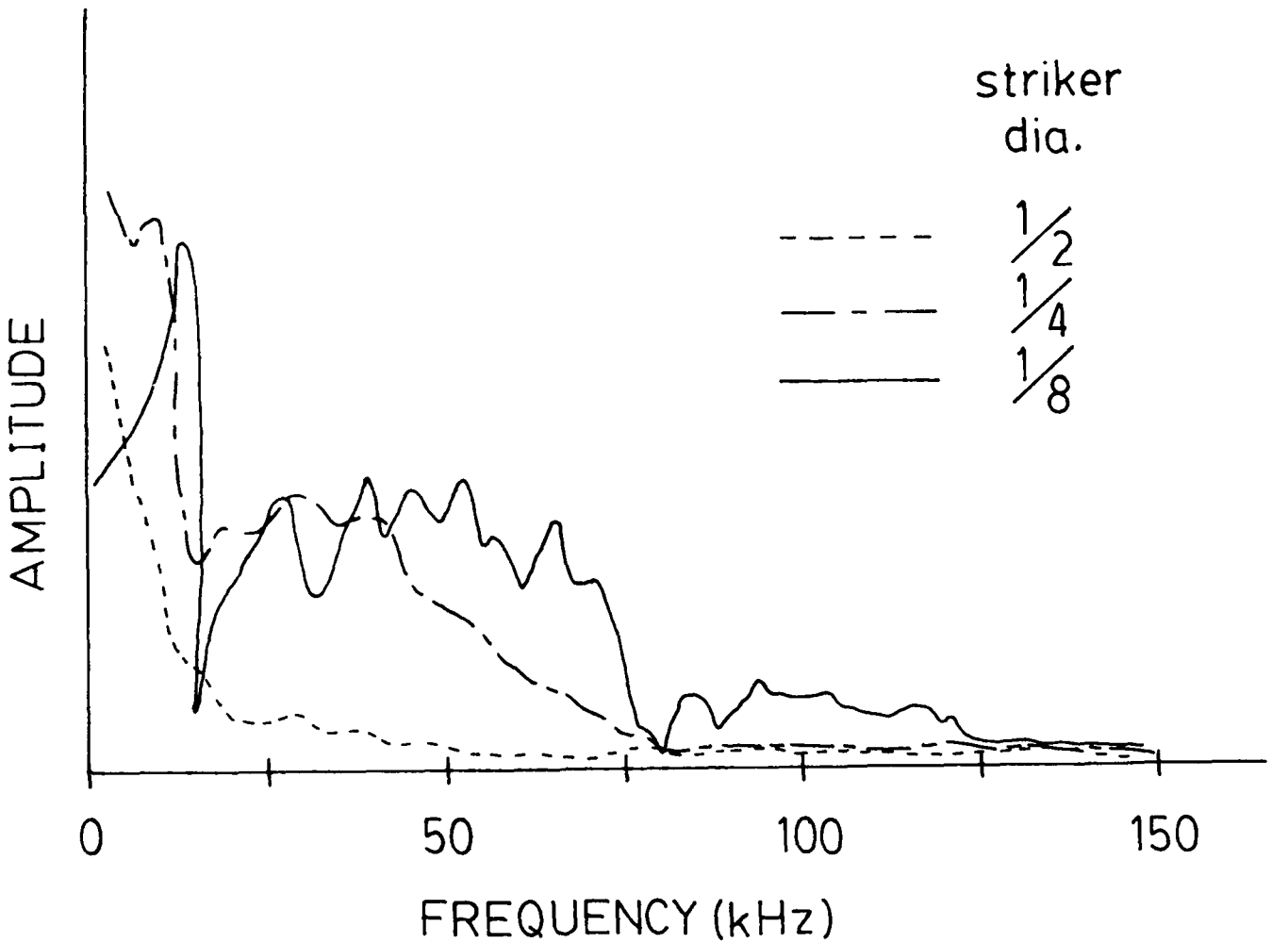

3.10. Frequency domain representation of loading histories over debond in Figures 3.3 to 3.5.

striker momentum for the 1/2- inch (12.7-mm)- diameter striker. The discrepancy increased somewhat for smaller strikers and a corresponding check for the 1/8-inch (3.18-mm) striker showed that the impulse averaged 14.1% lower than the change in striker momentum.

Since the contact force between striker and target must always be compressive, no negative output is expected from the transducer if it is viewed strictly as a contact load transducer. The "ringing" which appears in all of the experimental records subsequent to the main pulse appears to be associated primarily with an "accelerometer" type of response by the transducer arising from its mass and (high) stiffness. Also, as demonstrated previously[3,4] with this type of transducer, it is possible, even with the double crystal device, to produce output which is evidently associated with extraneous modes of (transducer) deformation, i.e., modes other than that of normal compression which is utilized for transduction. Early in the program, it was observed that tests with the 1/2-inch (12.7-mm) diameter transducer produced greater ringing than the 1/4-inch (6.35-mm) diameter transducer. Since Equation 1 indicates that the acceleration response (for transducers with the same element thickness) will be substantially independent of diameter, evidently the smaller transducer is less affected by motion in extraneous modes. For this reason, all subsequent data have been collected using the smaller transducers. For like experimental conditions, only slight differences are observed

between records obtained using the two different 1/4-inch (6.35-mm)-diameter transducers.

The reproducibility of the results is considered reasonable. For example, for a test series of two drops each at six locations with y = 1/2-inch (12.7-mm) on the aluminum plate with the 1/2-inch (12.7-mm)-radius debond, the average difference in two pulse peaks from the same station was 4.2% (S.D. = 3.196). These variations increased somewhat as striker size was decreased. For duplication of a test series incorporating five locations 1/2-inch (12.7-mm) from the edge of the fiberglass-epoxy plate (with a lapse of approximately four months between experiments) the average difference between comparable pulse peaks was 7.9% (S.D. = 4.5). These results indicate that some (increased) uncertainty is associated with coupling the transducer to the target.

In comparing force histories from debonded and well-bonded regions, records from both the aluminum and fiberglass-epoxy targets evidence an effect of the debond. Generally, the peak amplitude is lower over the debond and the pulse shape is more complicated. Furthermore, the transition in pulse character is closely associated with the transition from debonded to a well-bonded site. See, in particular, Fig. 3.4. Figs. 3.3 to 3.5 show that, for the 1-inch (25.4-mm)-radius debond, shorter loading durations (associated with smaller strikers) elicited relatively more change in response. For this reason, the 1/2-inch (12.7-mm)-radius debond was only interrogated using the smallest striker.

For the targets described above, all flaws have been associated with significant changes in transducer output, as compared to otherwise similar signals from unflawed regions. Preliminary tests on a recently fabricated aluminum target similar to those described above indicate that, for the present transducer configuration, transducer outputs associated with edge flaws of 1/4-inch (6.3-mm)-radius are differentiable from similar records from unflawed regions. For a 1/8-inch (3.2-mm)-radius flaw, our (as yet only qualitative) examination of comparable data indicates no significant differences between flawed and unflawed results. Resolution limits of this magnitude are not unexpected, as the plan dimension of the flaw here is of the same scale as both the target thickness and the transducer dimensions.

The spectra obtained from the 1-inch (25.4-mm)-radius debond between aluminum plates (Figs. 3.9 and 3.10) show a near discontinuity in the neighborhood of 14 kHz for the two smaller strikers. Furthermore, although such a discontinuity is not apparent in the spectrum of the load history for impact over the debond with the 1/2-inch (12.7-mm)-diameter striker, the maximum discrepancy between spectra in the presence of and away from the debond likewise occurs at about 14 kHz for this case. In view of the absence of any such notable features in the spectra for tests at well-bonded sites, this signature is taken to indicate the flaw presence. The fact that it is associated with a particular frequency strongly suggests that this frequency is associated with the size of the flaw.

If the flaw is modeled by a semicircular plate of the thickness of one of the bonded plates and considered clamped on its semicircular boundary, then the natural frequencies associated with the first several modes of vibration may be calculated.[3.5] The lowest natural frequency for such a plate is found to be 6.1 kHz, and the next resonance (associated with one nodal diameter) occurs at approximately 15 kHz. The fact that, even with such a highly oversimplified model, these frequencies are found to be in the same range as the particular spectral features noted above strongly supports the conlusions that these features are flaw specific. Furthermore, it suggests that this apparent signature of the flaw may ultimately be useful in determining flaw dimensions.

In view of the increasingly broad spectra associated with decreasing pulse durations, it is clear that shorter pulse length, associated with smaller strikers, is a desirable feature. This is consistent with the increased definition of flaws afforded by smaller striker loading which was noted earlier.

In conclusion we note that several parameters associated with the force histories might be considered as flaw indicators, e.g., peak force, net impulse, pulse shape and spectral characteristic(s). Of these the net impulse appears to be unsatisfactory (as can be seen by examining the area under curves in Figs. 3.3 to 3.6). Pulse peak and shape both exhibit distinguishable differences between records from unflawed and flawed locations. However, at the present

stage of our investigation, it appears that the frequency plane representation of the loading history provides the best opportunities for both flaw detection and characterization.

3.6 Acknowledgment

The authors acknowledge the able assistance of Mr. Imre Szauter, a former student at The Ohio State University, in conducting the experiments. This work is supported by USAF Contract F33615-8[illegible]K-5009; Dr. Robert L. Crane of the Air Force Materials Laboratory is the contract monitor.

3.7 References:

3.1. Hagemaier, D.J., "Bonded joints and non-destructive testing 1. Bonded honeycomb structures," Non-destructive Testing, v. 4, pp. 401-407, December 1971.

3.2. Schliekelmann, R.J., "Non-destructive testing of adhesive bonded metal-to-metal joints 1," Non-destructive Testing, v. 5, pp. 79-86, April 1972.

3.3. Schliekelmann, R.J., "Non-destructive testing of adhesive bonded metal-to-metal joints 2," Non-destructive Testing, v. 5, pp. 144-154, June 1972.

3.4. Kenner, V.H., "On the Use of Quartz Crystals in Dynamic Stress and Force Transducers," Experimental Mechanics, v. 15, pp. 102-106, 1975.

3.5. Khurasia, H.B. and Rawtani, S., "Vibration Analysis of Circular Segment Shaped Plates," Journal of Sound and Vibration, v. 67, pp. 307-313, 1976.

4. Quantification of the "Tapping" Technique for the Detection of Edge Defects in Laminated Plates

by

Vernal H. Kenner, George H. Staab and Hung-Sying Jing

Department of Engineering Mechanics
The Ohio State University
Columbus, Ohio 43210

4.1 Abstract

A miniature piezoelectric transducer has been used to sense both details of the loading history and features of the ringing response in tapping tests conducted on bonded aluminum and graphite epoxy plates which contained artificial flaws. Either the loading or the ringing phase of the resulting output records exhibit significant differences for loading occuring over as opposed to off of the flaw. When the data are examined in the frequency domain, it is found that major details are beyond the audible range of frequencies.

4.2 Introduction

The practice of lightly tapping various bodies to gain information about unseen structural details is widespread. As an everyday example we note that the location of studs behind plasterboard walls is routinely accomplished by this means. Another ordinary example is provided by the method commonly used to evaluate the seal between lid and bottle in home canning operations; this consists of lighly tapping the lid with, say, a spoon and evaluating the consequent sound. The application of the tapping technique in structures of greater sophistication and, in particular, those utilizing adhesive bonds is also widely practiced. The tapping technique is discussed in several review articles on the non-destructive evaluation of bonded structures.[4.1-4.2]

As practiced in its basic form, the tapping method relies exclusively on the ability of an inspector to "hear" the difference between an acceptable and an unacceptable bond or delamination. The shortcomings of such a qualitative procedure are well understood. Devices for improving the tapping test are described in References 4.1 and 4.2; these improve both the control of the mechanical energy comprising the test input and electromechanical amplification and (in one case) measurement of the structure's response.

The present interest in the tapping technique is directed toward the in-service detection of edge flaws in adhesive joints and composite panels. This interest is motivated by the following

considerations: 1. In-service flaws usually occur at boundaries, both because, typically, stresses are highest and because bond degredation due to contamination by e.g., moisture absorption, occurs at edges. 2. While ultrasonic inspection techniques under ideal (laboratory) conditions have been able to detect flaws down to approximately 3mm in diameter in graphite-epoxy composite panels[4.3], the necessary techniques, including water immersion, do not lend themselves to in-service tests. Furthermore, the edge locations of normal in-service flaws are the locations where ultrasonic techniques often are found to be inadequate.

The tests presently described revolve around the use of a miniature force transducer to measure changes in force histories resulting from the controlled impact of dropped steel spheres onto targets which consisted of both bonded aluminum plates and graphite-epoxy panels. These targets all incorporated artificial flaws. While the tests permitted the observation of ringing subsequent to the impact of the steel spheres with the targets, along the lines of the usual tapping test, they also provided a direct measurement of the modification to the impact force history induced by the presence of a flaw.

In order to elicit a response associated with the small flaws of interest relatively high frequencies need to be present in the exciting event. While several instrumented hammers are commercially available which contain accelerometers and/or force transducers, these devices will both generate and be responsive to frequencies

lower than those of interest here. Furthermore, in this study, which was directed more toward an understanding of the phenomena of an impact type test rather than the application of such a technique per se, it was desirable to have highly repeatable inputs, which are reasonably attainable with a drop type test. Further, in this research setting, the ball drop procedure provides quite precisely a known mechanical input, namely, the initial momentum, and thus circumvents calibration difficulties which would be inherent with an electromechanical device such as an ultrasonic transducer (which may well move superior in an application setting, however).

4.3 Procedure

Both aluminum and graphite-epoxy composite targets were examined in the present study. The former specimens were fabricated by bonding two 254 x 508 x 2.03-mm (20 x 10 x 0.080-inch) 2024-T4 aluminum plates together with FM-73M (American Cyanamid, Havre de Grace, Maryland) structural adhesive. This adhesive includes skrim cloth, is obtained in a roll, and produces a final bond thickness of approximately 0.08 mm (0.003-inch) after curing at elevated temperatures with clamping pressure according to the manufacturer's instructions. This was accomplished by placing the target lay-up between two teflon-coated steel plates which were drilled around their perimeter to accommodate bolts through which clamping pressure was applied. The combination of spring-washers under the clamping bolts and torque-wrench controlled tightening was found to yield satisfactory targets. Artificial flaws

of semicircular shape centered on the long edge of the targets were created by inserting a suitably shaped piece of a thin polymeric film (Kapton) which was approximately 0.010-mm (0.0004-inch) thick between the adhesive layer and one of the aluminum plates. Three such flaws in two aluminum targets were tested; these flaws had radii of 50.8 mm, (2-in), 25.4 mm (1-inch) and 12.7 mm (1/2-inch), respectively. As detailed elsewhere[4.4], destructive tests on small samples cured as described above showed that satisfactory, void free bonds were produced by this procedure.

The graphite epoxy targets were fabricated from an AS4/3502 system (Hercules, Magna, Utah) supplied as a 152.4 mm (6-inch)-wide prepreg tape. Two targets nominally 450 x 203 x 2.8-mm (17.75 x 8 x 0.11-inches) consisting of twenty alternating $0^{o}/90^{o}$ plies, symmetric about the mid-plane, were made. A third panel nominally 305 x 152 x 2.8-mm (12 x 6 x 0.11-inches) was also fabricated. Semi-circular defects of 50.8 mm (2 inch), 25.4 mm (1 inch), 12.7 (1/2 inch) and 6.35 mm (1/4 inch) radius were placed in these specimens by inserting two Kapton layers between the middle plies during the lay-ups. These targets were cured in the plate fixture described earlier at a temperature of $190^{o}C$ for a period of approximately 3 hours. Since our apparatus did not provide for "bleeding" of the epoxy, the resulting panels were epoxy rich.

The minature force transducer used in all of the present tests utilizes two 6.35-mm (0.250-inch)-diameter X-cut quartz crystals to

eliminate bending contributions[4.5]. These are interspersed between three 0.51-mm (0.020-inch)-thick brass electrodes. A 1.25 mm (0.50-inch)-thick metal protector disk, wrung to the double crystal transducer with the aid of a small amount of grease, provides the surface upon which the striker impinges. The general characteristics of such load transducers are described elsewhere[4.5]; the particular design used in this study was selected from several possibilities previously examined for debond detection[4.4].

The flawed panels were clamped, at the edge opposite that containing the flaw, to an x-y stage which permitted positioning to within 0.25-mm (.001-inch). Steel spheres of 3.175-mm (0.125-inch) and 6.35-mm (0.25-inch)-diameter were dropped a distance of 59 mm (2.31 inch) from a drop fixture which held the striker until release by means of orally applied suction. The drop fixture was in turn supported by a dial indicator stand which was magnetically afixed to a massive steel surface. The x-y stage was bolted to this surface as well. A miniature plumb bob was constructed to hang from the drop fixture for close location of the impact site. For reasons described below some additional tests were carried out in which the double crystal transducer was not struck directly but placed at 12.7mm (1/2-inch) away from the impact site, which was covered by a hardened steel protector identical to that wrung atop the transducers. A schematic of the apparatus is given in Fig. 4.1.

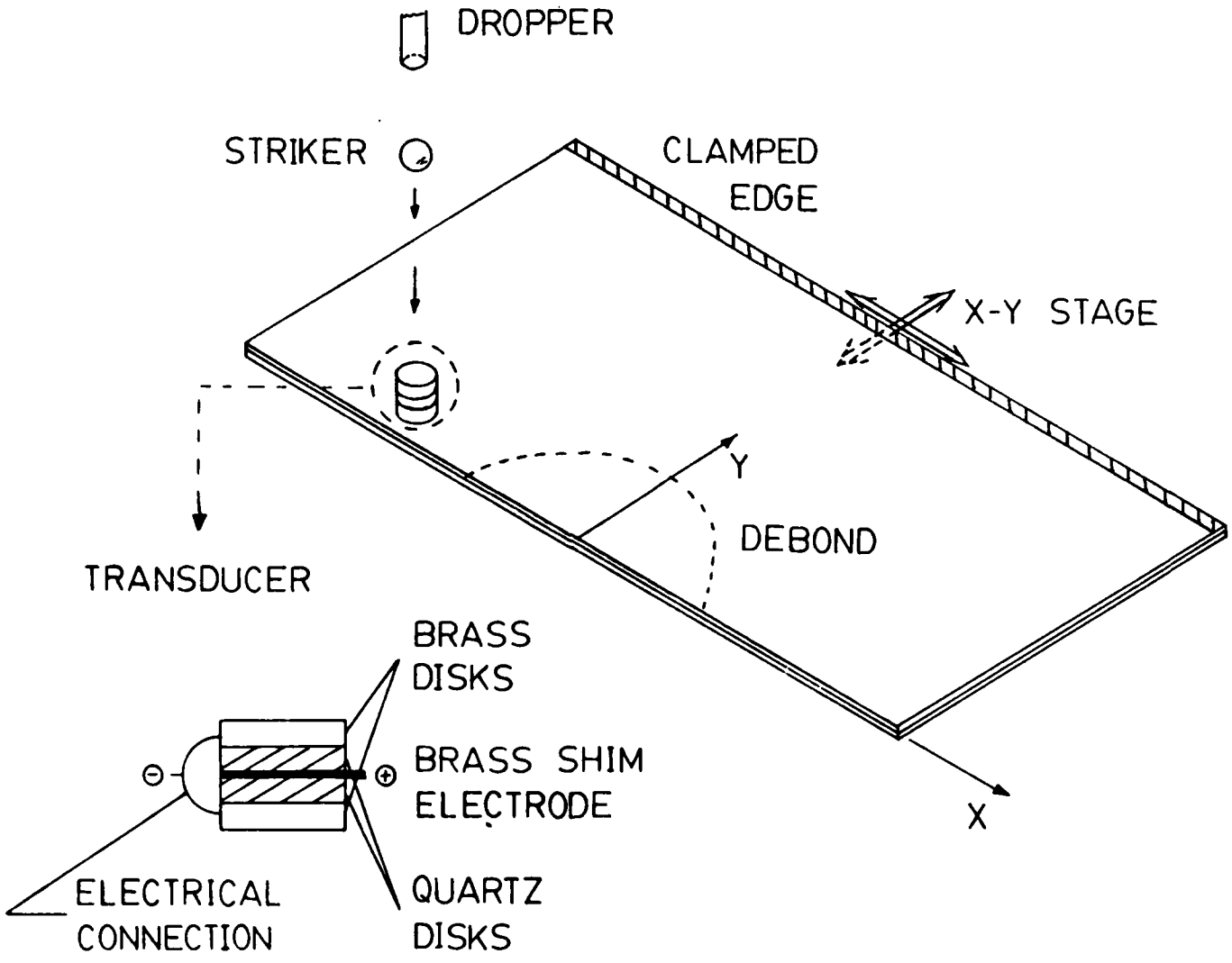

4.1. Schematic of the apparatus.

The above efforts notwithstanding, it was found that to assure the best repeatibility from run to run with the smallest strikers additional precautions were necessary. First, it was found that both steel and aluminum protector disks were minutely dented by the hardened steel strikers, even at the low impact velocities employed. This produced some randomness in the test results which we attributed to variations in the impact surface properties due to localized work hardening associated with prior impacts. Thus, the protector disks ultimately employed were machined from drill rod, hardened, and then ground. Second, it was found that very small amounts (i.e., only indriectly detectible) of grease or oil present on either the 3.175-mm (0.125)-inch)-diameter strikers or the protector disk surface could substantially affect the force-time history. A procedure in which the spheres were washed in acetone, only dropped once before re-washing, and never touched by hand after washing and prior to dropping satisfactorily eliminated this problem.

A capacitor was placed in parallel with the double crystal transducer to suitably extend the long-time frequency response of the circuit[4.6]; the total circuit capacitance was measured with an impedence bridge and found to be 2.07 nF. The crystal output was fed directly into a digital oscilloscope (Nicolet Instrument Co.) which recorded two points per microsecond for a duration of 512 s. This record was then stored on a 5 1/4-inch floppy diskette contained in a disk drive integral to the oscilloscope main frame. In turn,

such records were transferred via an IEEE-488 interface to our MINC-11 laboratory computer (Digital Equipment Corp.), where permanent storage of records was made on a 8-inch floppy disks utilized by this unit. A fast Fourier transform was used to calculate the Fourier magnitude spectrum.

4.4 Results

Fig. 4.2 presents transducer outputs obtained from the aluminum targets for loading by the 3.175 mm (0.125-inch)-diameter striker both over and removed from the flaw. Fig. 4.3 presents similar results for the graphite-epoxy targets. In these plots the x-y coordinate system referred to is that defined in Fig. 4.1. The peak voltages observed while traversing the flaws at a fixed distance, y = 6.35 mm (1/4-inch) in from the specimen edge are shown in Fig. 4.4 for the aluminum and graphite-epoxy targets, respectively. Fig.4.5 is a similar plot of results obtained while traversing the 50.8-mm (2-inch) radius flaw between aluminum plates along the line y = 0, perpendicular to the edge of the plate; results for both 3.175 and 6.35 mm (0.125 and 0.25-inch)-diameter strikers are presented.

Magnitude spectra are plotted in Figs. 4.6 and 4.7 for flaws in the aluminum and graphite-epoxy targets, respectively. These spectra are based on the entire record duration of 512 microseconds.

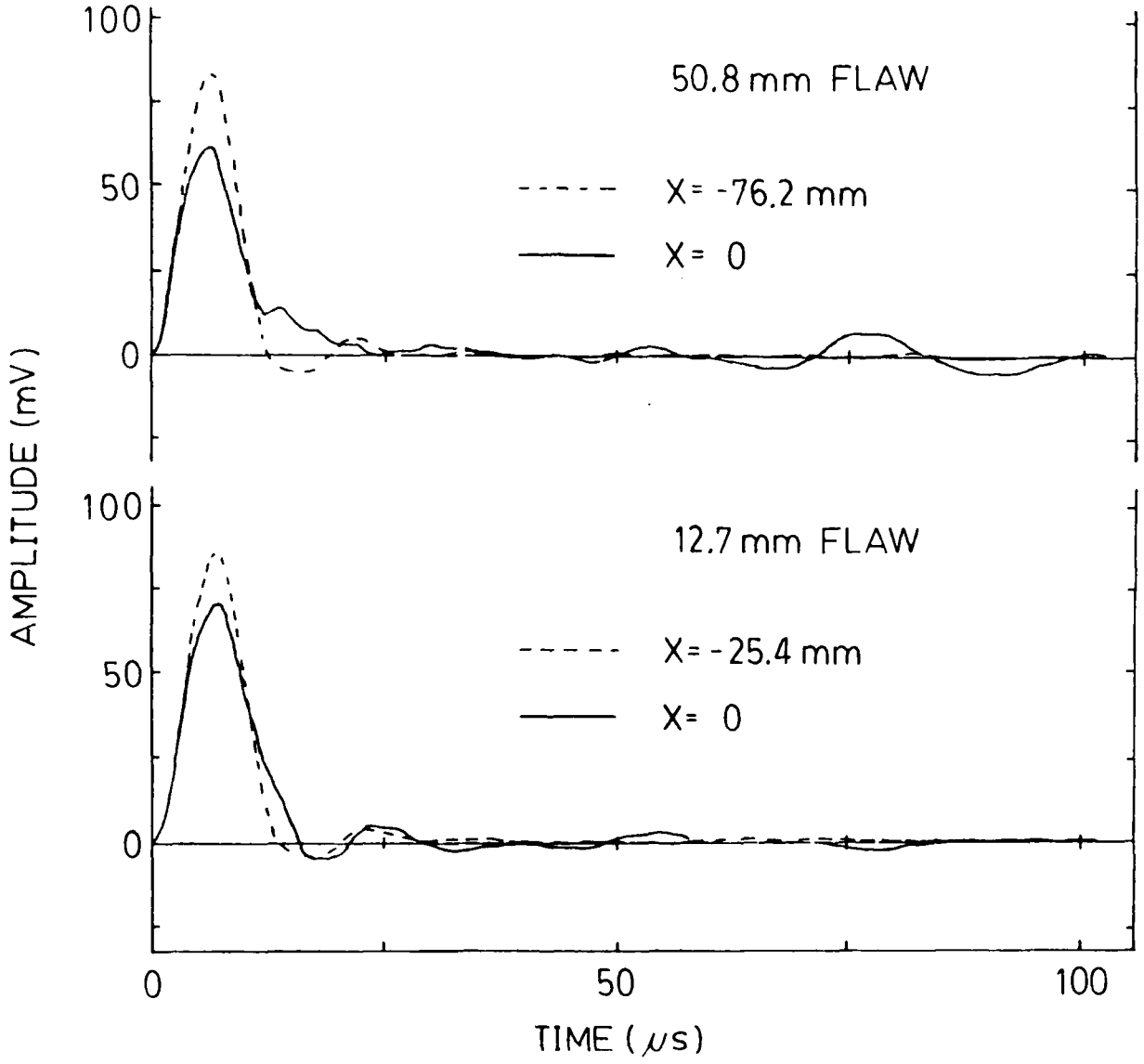

4.2. Transducer outputs from bonded aluminum targets for y = 6.35 mm.

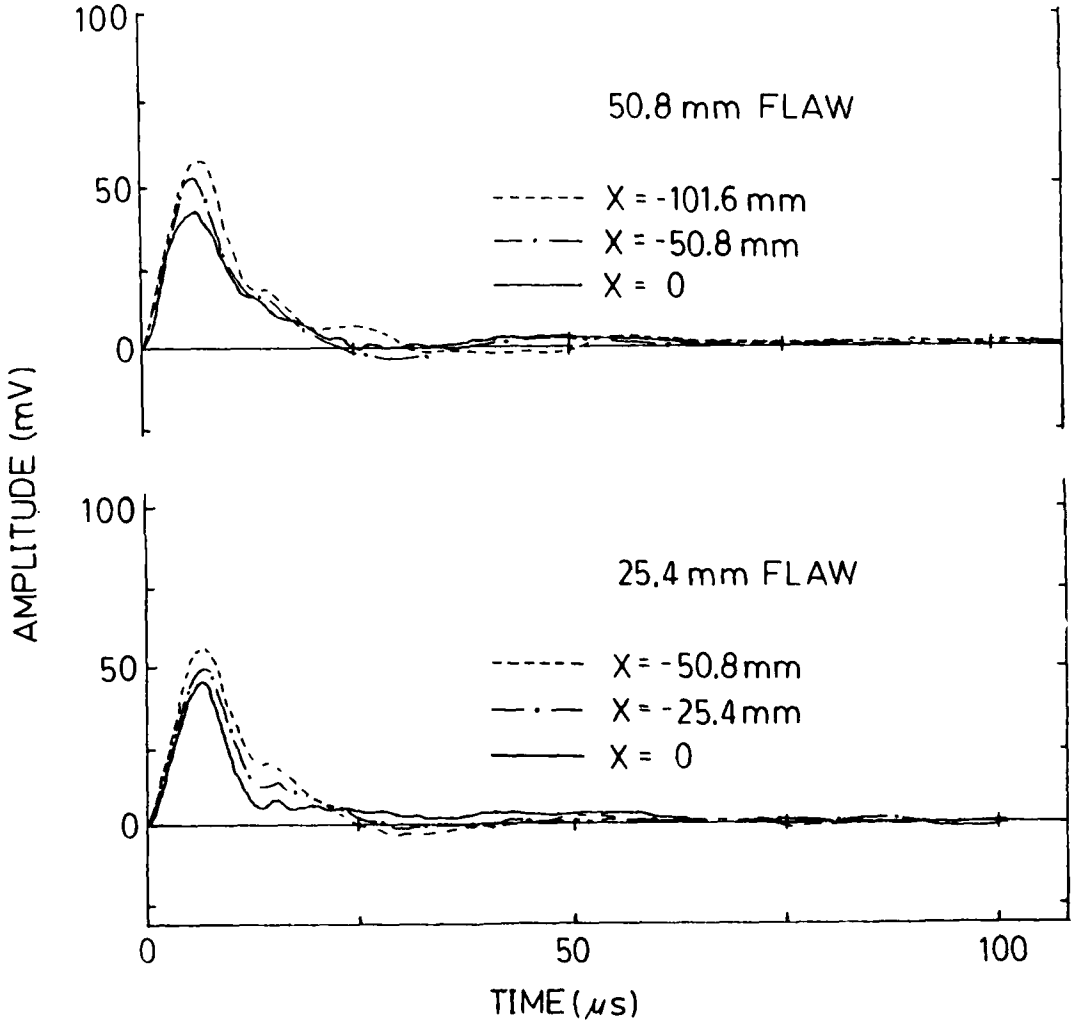

4.3. Transducer outputs from graphite epoxy targets for y = 6.35 mm.

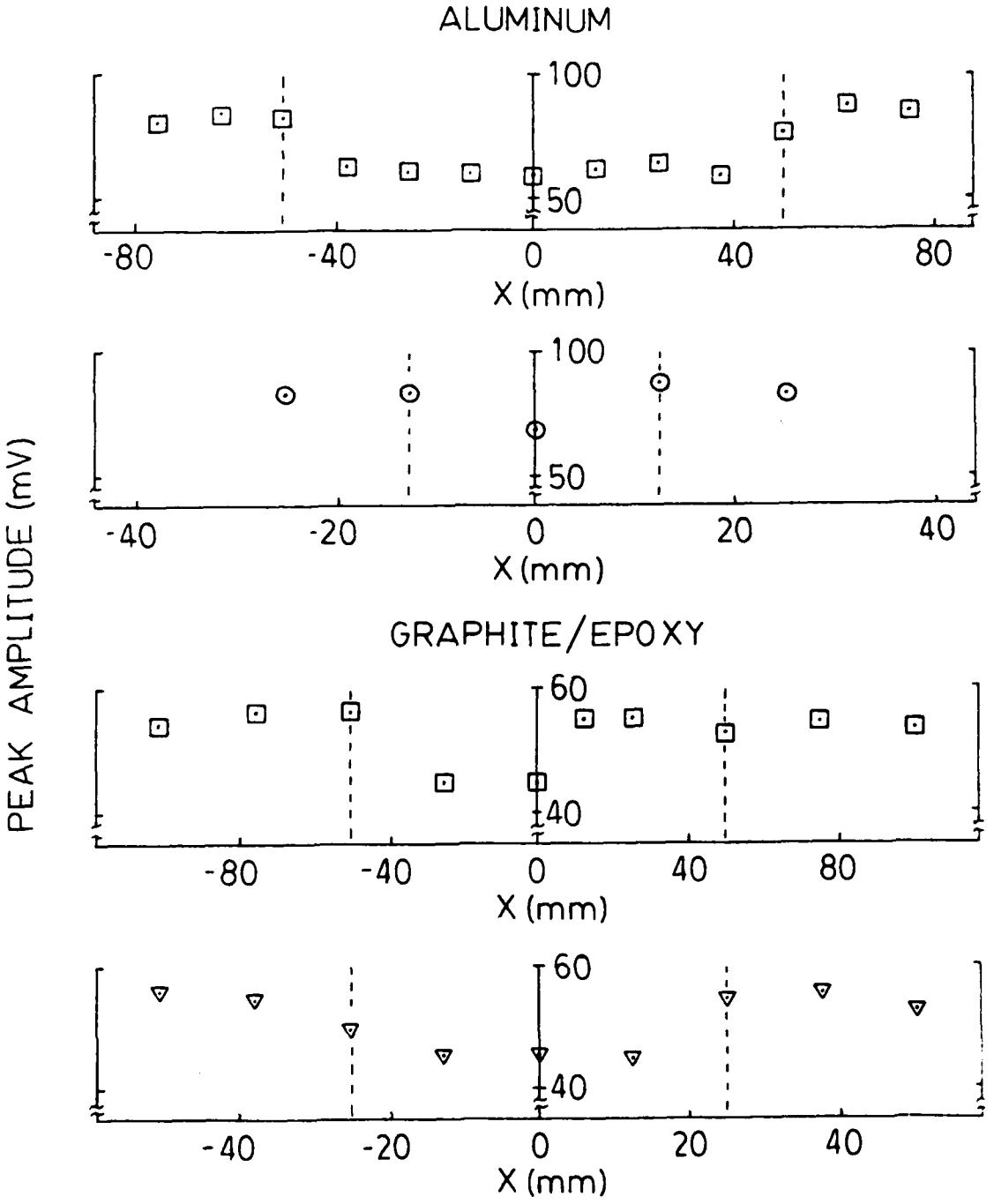

4.4. Transducer peak output (mV) for y = 6.35 mm. Vertical dashed lines represent the nominal flaw boundaries.

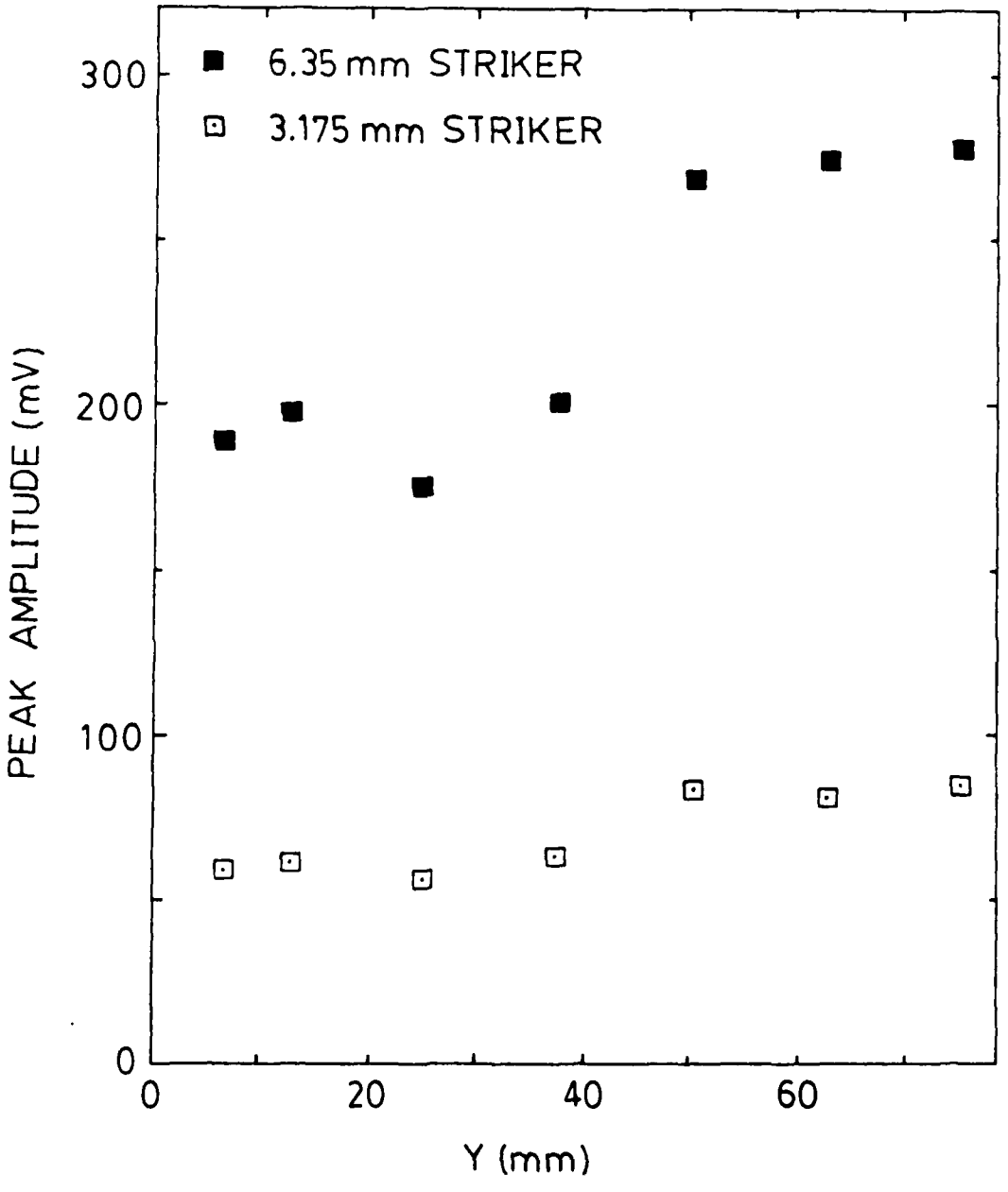

4.5. Transducer peak output vs. distance from the target edge for the 50.8 mm-radius flaw between aluminum plates, x = 0.

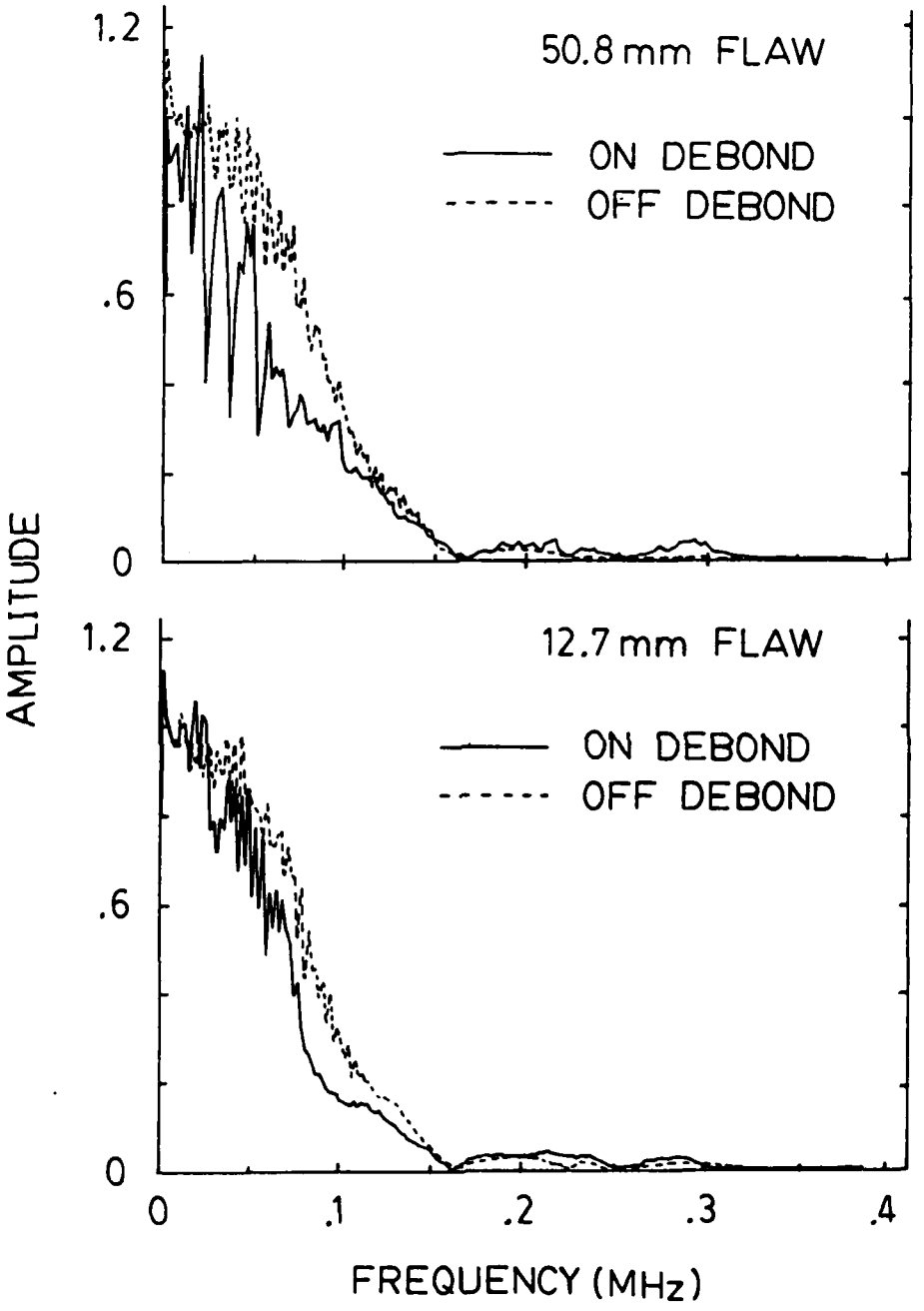

4.6. Magnitude spectra from aluminum targets (corresponding to Figure 4.2).

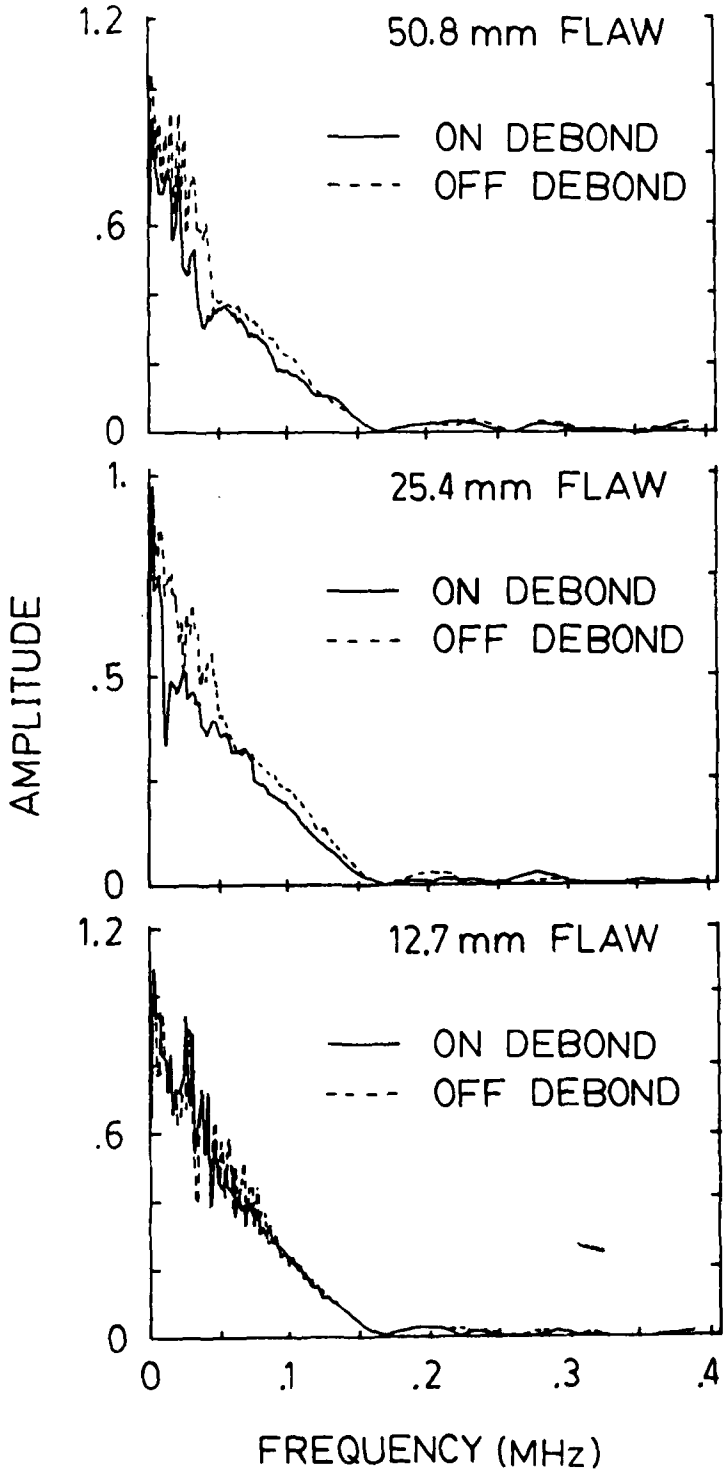

4.7 Magnitude spectra from graphite epoxy targets (corresponding to Figure 4.3).

4.5 Discussion

The transducer utilized in our experiments was initially developed to measure transient dynamic forces, as those arising during the loading portion of the present tests[4.5]. In that capacity it has proved acceptable; the observed change in striker momentum and the impulse measured by double crystal transducers is typically found to be within 10%. In the present tests the double crystal transducer is also utilized as an accelerometer which records the ringing of the target subsequent to the impact. During the impact portion of the test the transducer outpout voltage is thus associated with the striker contact force through the formula[4.5]

$$F(t) = \frac{CV(t)}{2k}$$

where C is the circuit capacitance (2.07 nF), k is the appropriate piezoelectric constant (2.3×10^{12} coulombs/newton), and V(t) and F(t) are the time-dependent output voltage and contact force, respectively. Subsequent to actual contact the transducer output may be associated with acceleration by dividing F(t) by an appropriate mass. A reasonable first approximation of that mass could be that of that portion of the transducer above the plane separating crystals and including the hardened steel protector. Since in the present application the actual values of forces or accelerations is not necessary, neither of the above calculations were made.

One possible means of flaw identification would be to detect changes in peak pulse amplitude associated with the flaw. As shown in Fig. 4.4, this would be possible for all the flaws studied in the aluminum targets. While the decreases in peak amplitude are relatively modest, 27% and 18% for the 50.8 mm and 12.7 mm (2-inch and 1/2-inch)-radius flaws, these differences are nonetheless significant when compared to the usually observed experimental variation. For example, the average standard deviation for three tests making up one of the points in the first plot shown in Fig. 4.4 is 1.6 mV, corresponding to 1.9% of the peak. For the graphite-epoxy samples (Fig. 4.4), 25.4 mm (1-inch) and 50.8 mm (2-inch) radius defects likewise produced a significant decrease in peak amplitude (29% and 27%, respectively) when loading occured over the flaw, but the changes in this parameter for tests of the 12.7 mm (1/2-inch)-radius flaw were not significant.

In three instances, records obtained from the transducer were not as anticipated. For the case of the 50.8 mm (2-inch)-radius flaw in the graphite-epoxy plate the record of peak output clearly suggests that the right-hand edge of the flaw is located near x = 12 mm (0.5-in), and not at x = 50.8 mm, as expected. For the 12.7 mm (1/2-inch)-radius flaw, while there is no clue to the flaw's presence contained in the peak amplitude data, significant spectral differences did exist, as described below. However, in an earlier panel which was fabricated to contain a flaw of this size, no

evidence of the flaw was observed in an interval 101.6 mm (4-inches) long centered at x = 0, the presumed flaw center. In this case the panel was cut into 6.3-mm (1/4-inch) squares in the rectangular region $0 < y < 12.7$ (mm) and $-50.8 < x < +50.8$ (mm). No evidence of a flaw was observed, indicating that either the flaw was inadvertently cut away during machining to trim the panel prior to testing or sufficient flow of the epoxy matrix occurred between the Kapton sheets during the curing cycle to bond them together. Either possibility was enhanced by the fact that this was the first graphite-epoxy target fabricated and both cure temperature and pressure were somewhat excessive. On the other hand testing of the 25.4 mm (1-inch)-radius flaw between bonded aluminum plates yielded a peak signal amplitude vs. location along the line y = 12.7 mm (1/2-inch) shown in Fig. 4.8. In view of the clear indication given by this figure that the flaw extended well to the left of the edge of the artificially contrived defect, (to about x = -65 mm at depth y = 12.7 mm), this plate was also sacrificed into 12.7 mm (1/2-inch) squares. The debonded area indicated by the peak amplitude rate was verified. Indeed, upon intermediate sectioning it was discovered that there were residual stresses tending to separate the aluminum surfaces; these stresses were manifested by warping of the strips and concomitant debonding of the strips remaining outside of the zone reduced to squares. Thus, in two cases where the transducer outputs have suggested a bonding condition other than expected,

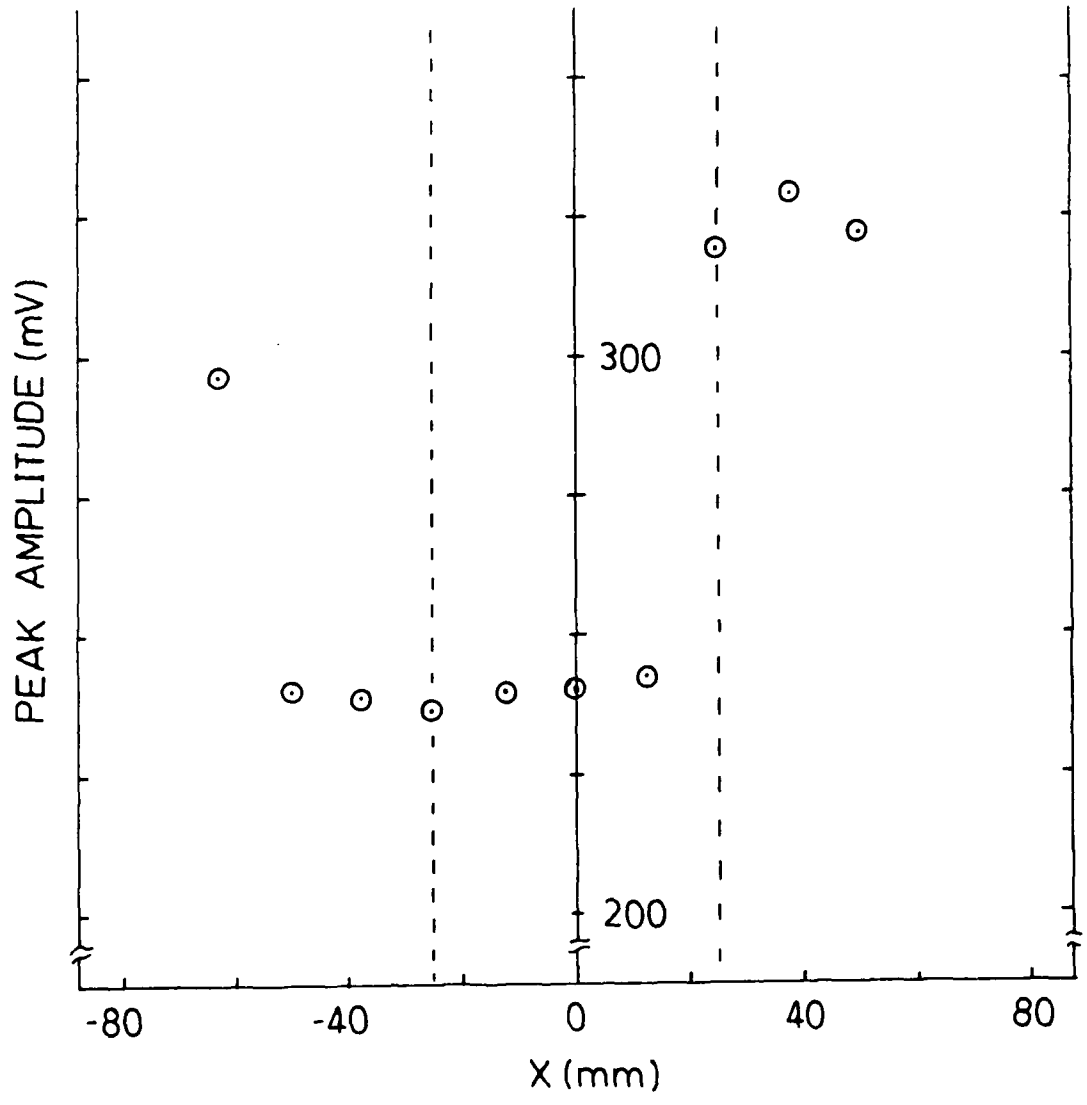

4.8. Transducer peak outputs for y = 12.7 mm, bonded aluminum target, nominal 25.4 mm-radius flaw. Vertical dashed lines represent the nominal flaw boundaries.

sectioning of the panels has verified the abnormality. We have not yet sacrificed the graphite-epoxy panel containing the 50.8 mm (2-inch) radius flaw because of anticipated additional tests.

The amplitude spectra of Fig. 4.6 for tests on the 12.7 mm (1/2-inch)-radius debond and the 50.8 mm (2-inch)-radius debond in the aluminum targets show clear differences between the results of interrogation over or away from the debond. For example, the spectrum is seen to fall more rapidly with increasing frequency for impact over the debond than it does for impact off of the flaw. The spectrum is generally rougher for on-debond loading. For the 12.7-mm (1/2-inch) radius flaw, the sharp discontinuity at approximately 30 kHz is reminiscent of a similar feature exhibited by spectra obtained from the 12.7 mm (1-inch) radius flaw in the aluminum target reported earlier[4.4]. The discontinuity in this case occurred at a frequency of approximately 14 kHz. For the loading over the 50.8 mm (2-inch)-radius flaw the differences described above are accentuated, with multiple sharp discontinuities observed in the frequency spectrum. We note here that there is little difference in the off-flaw records shown in Fig. 4.6. Thus the presence of a flaw near, but not under, the transducer appears to have little effect on the spectrum obtained.

Recognizing that there is little apparent difference between the actual loading, or primary peak, portion of records obtained over or off of the debond, the Fourier analysis was carried out

selectively over several intervals characteristic of all records. The first interval (impact) consisted of the primary, compressive portion of the record up to the first base-line crossing (Figs. 4.2 and 4.3). A second interval (ringing) was defined as following the first base-line crossing and continuing to the time when significant oscillations associated with the return of flexural waves from the back and side boundaries of the panel appeared in the record. While spectra (not shown) limited to the impact interval are essentially the same for on-and off-debond tests, spectra (Fig. 4.9) from the ringing interval show substantial differences depending upon transducer location. Thus it seems clear that the changes in spectral detail (Fig. 4.6 and 4.7) occurring when loading is over a debond are associated primarily with the ringing, and not the initial impulse portion. Furthermore, by exmaining only the ringing portion of the records the spectral differences between on-debond and off-debond loading are accentuated (Fig. 4.9).

The spectral features illustrated above by results from aluminum targets were also observed to occur for flaws in the composite panels. Fig. 4.10 presents ringing spectra from the three flaws located in graphite-epoxy targets. While significant differences exist in this case between on-flaw and off-flaw ringing spectra, there is considerably less difference in the amplitude of the higher frequency (f ~ 100 kHz) portions of the on-flaw compared to off-flaw spectra than there is for corresponding results with aluminum targets.

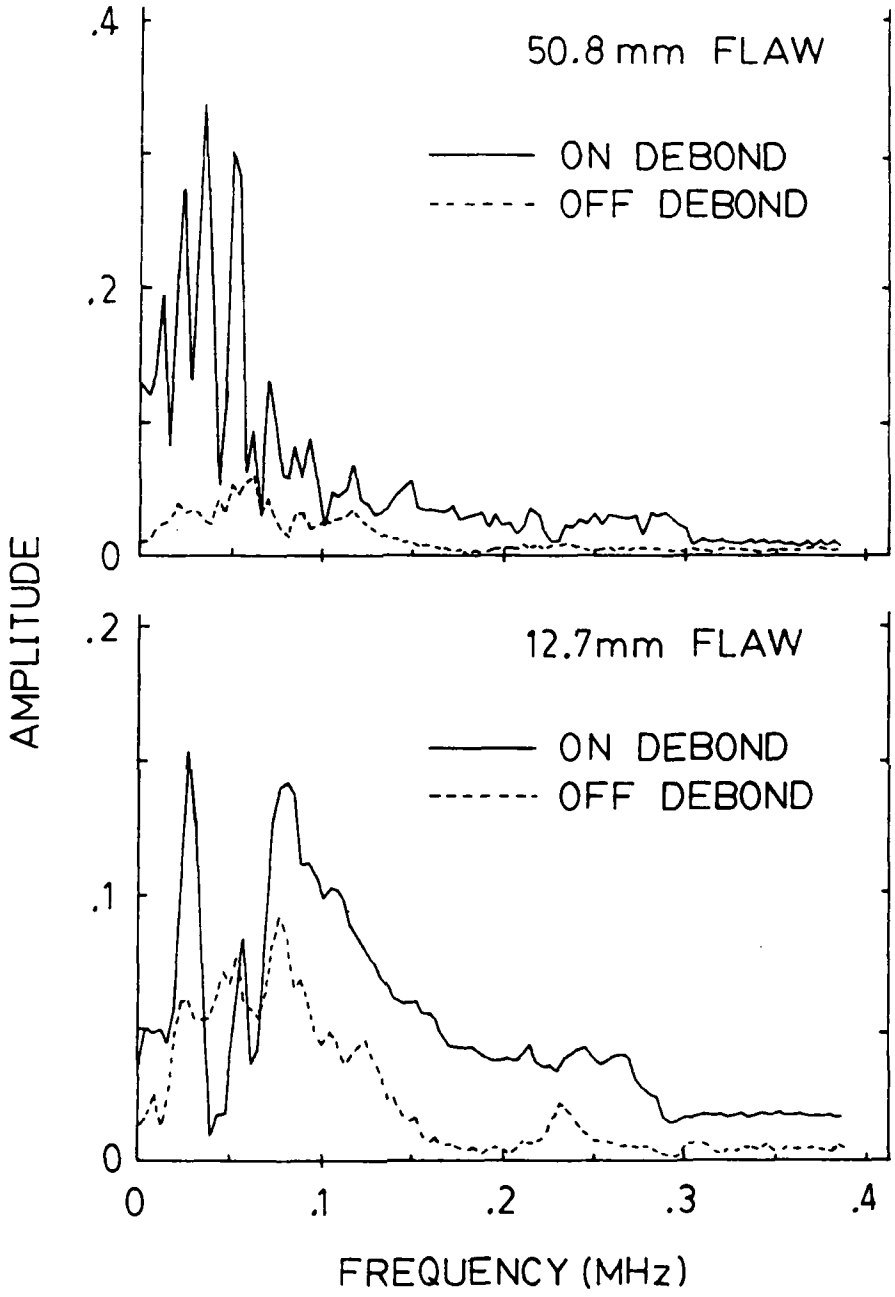

4.9. Ringing magnitude spectra for flaws in bonded aluminum targets.

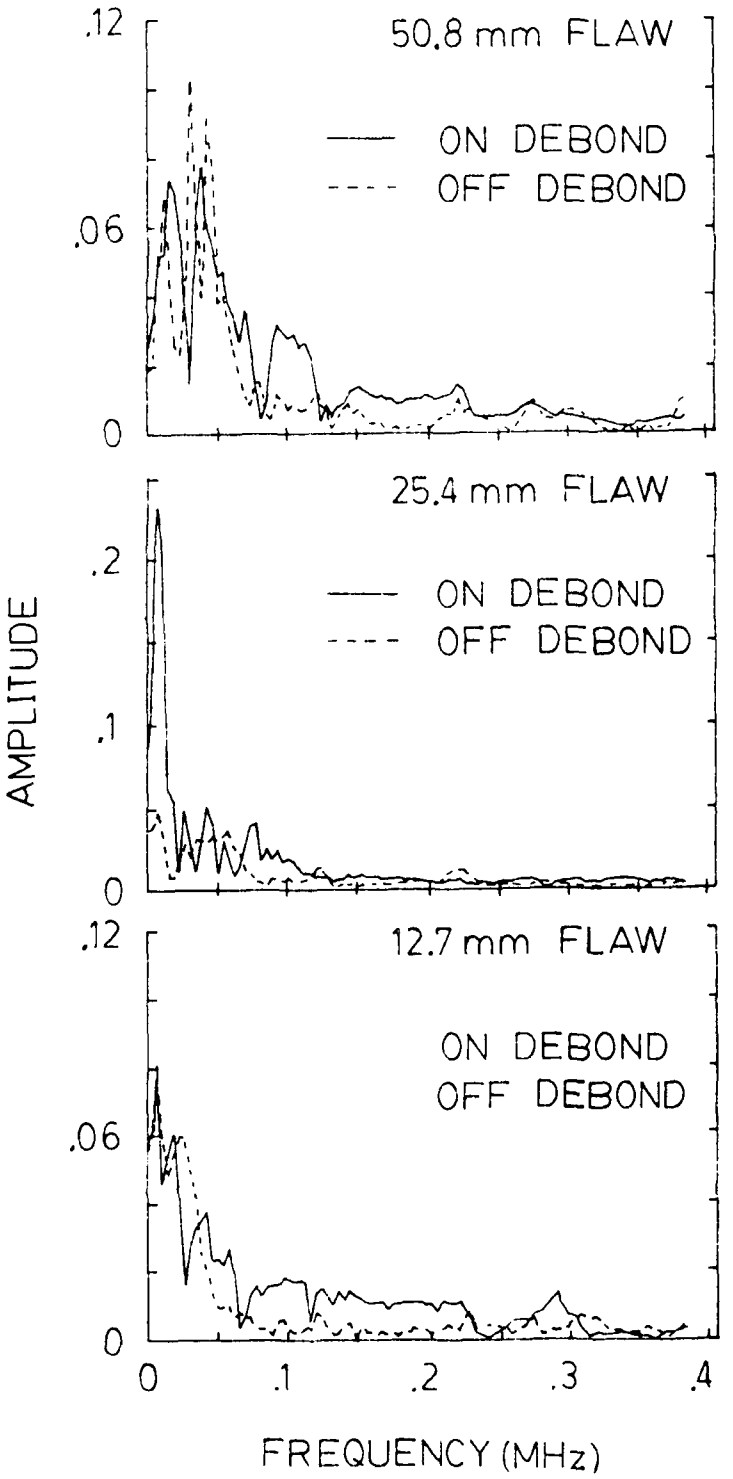

4.16. Ringing magnitude spectra for flaws in graphite epoxy targets.

In closing our discussion of the results of spectral analysis we observe that the frequency resolution (i.e., the inverse of the duration of the examined record[4.7]) is approximately 2 kHz when the complete transducer output record is analyzed (Figs. 4.6 and 4.7). For the smaller durations analyzed to produce Figs. 4.9 and 4.10 the resolution is increased to about 4 kHz. These resolution levels comprise a relatively large fraction of the entire frequency range in which the human ear can discern a change in frequency - from about 10 Hz to 20 kHz typically and 30 kHz, at most[4.8]. Thus, our results are limited insofar as evaluating the audible output of a tapping test. However, the significant spectral details that we observe at frequencies in excess of the audible limit suggest strongly that, for the flaws under consideration here, limited information is available in the audible range. This is supported by the fact that very crude modelling of the flaw as a semi-circular, clamped plate leads to natural frequencies exceeding the audible range. For example, for the 12.7 mm (0.5-inch)-radius flaw between bonded aluminum plates, we have calculated, with the aid of a finite element model, that the lowest natural frequency is 24 kHz. This flaw would thus be undetectable to the typical human ear.

Guided by the observation that significant information was obtained when the transducer acted in its "accelerometer" mode, as opposed to its "force transducer" mode, an initially unanticipated series of tests was carried out where the transducer was not struck

directly and thus acted solely as an accelerometer. The advantage of this configuration lies in eliminating the direct impact portion of the transducer output from the experimental records. This permits much better observation of the relatively much smaller accelerometer response. In these tests, the striker was dropped on a hardened steel protector disk located at position (x,y + 12.7) (mm) while the transducer including its steel protector was located at position (x,y). The results of such a test for the 25.4 mm (1-inch) radius-debond in a graphite-epoxy target are presented in Fig. 4.11. For this test series the circuit capacitance was much lower, 208 pf. This has the effects both of increasing the output signal and of lowering the low frequency response.

In comparing Fig. 4.11 to Fig. 4.3, it is clear that the differences from on-flaw and off-flaw transducer outputs are accentuated in this test configuration. For such an indirect test on the second 12.7 mm (0.5-inch) flaw in a graphite-epoxy target the peak amplitude was lower by 18% over, as compared to off of, the flaw; as noted previously, this flaw produced no significant difference in peak transudcer output for the direct loading experiments. While we have yet to examine in any breadth the interaction of relevant parameters for this test configuration, it appears to offer increased sensitivity for flaw detection.

In closing this discussion, we comment on the effect that the plate clamping procedure has on the results. For these experiments

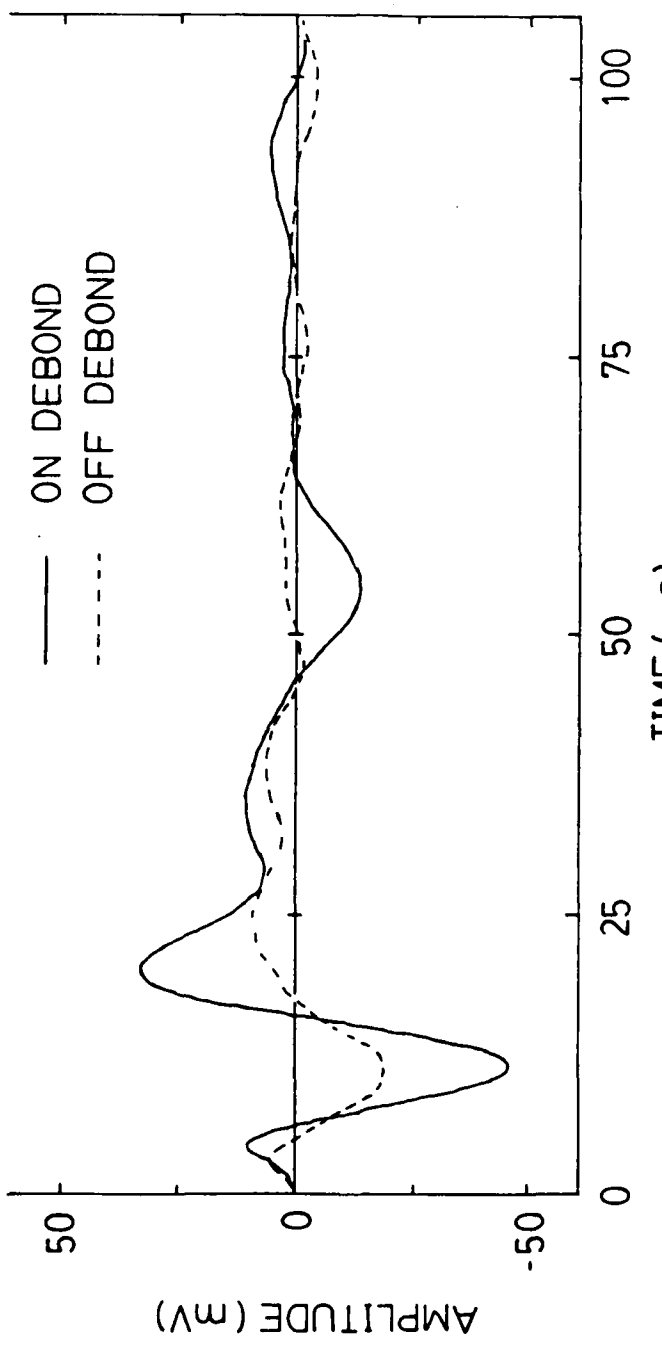

4.11. Transducer outputs for off-transducer loading at y = 12.7 mm, graphite-epoxy target, 25.4 mm-radius flaw.

the clamped boundary was usually roughly 200 mm (8 inches) from the flaw except for the smallest graphite-epoxy panel, for which this distance was about 125 mm (5 inches). In tests not presently described, flexural waves in the aluminum targets were found to propagate at 1780 m/s (70,000 in/s) while the corresponding values for the graphite epoxy were never greater than 1370 m/s (54,000 in/s). Thus, for the aluminum targets, boundary effects are not present until about 229 microseconds after impact while for the two larger and single smaller graphite epoxy targets corresponding times are 296 microseconds and 185 microseconds, respectively. For times less than these, the present results are unaffected by boundaries (other than that boundary intrinsic to the edge flaw). For times greater than these, and, more generally, for the various geometries and structural support conditions which might be encountered in service, boundary conditions would be expected to change the transducer output. This should only change what might be called the background signal; differences intrinsic to the presence of or absence of the flaw will still be contained in the record.

4.6 Conclusions

In a tapping test, information pertining to the existence of a flaw is contained both in the changes induced in the loading history and in the differences produced in the ensuing ringing. Either of these changes were of sufficient magnitude to provide flaw characterization in the present tests. For these tests, significant special features ere present above the audible frequency limit.

4.7 Acknowledgement

The authors acknowledge the valuable assistance of Mr. T. C. Harper in fabricating the apparutus. This work was sponsored by USAF contract F33615-82-K-5009; Dr. Robert L. Crane of the Air Force Materials Laboratory is the contract monitor.

4.8 References

4.1. Hagemaier, D.J., Nondestructive Testing, Vol. 4, Dec., 1971, pp 401-407.

4.2. Schliekelmann, R.J., Nondestructive Testing, Vol. 5, June, 1972, pp. 144-152.

4.3. Schramm, S. W., Daniel, I.W. and Hamilton, W.G. in Mechanics of Nondestructive Testing, W.W. Stinchcomb, Ed., Plenus Press, New York, 1980, pp. 309-324.

4.4. Kenner, V.H., Staab, G.H. and Jing, H.-S., Experimental Mechanics, in press.

4.5. Kenner, V.H., Experimental Mechanics, Vol. 15, March 1975, pp. 102-106.

4.6. Gurtin, M.E., Experimental Mechanics, Vol. 1, June 1961, pp. 206-208.

4.7. Bendat, J.S. and Piersol, A.G., Engineering Applications of Correlation and Spectral Analysis, J. Wiley and Sons, 1980, p. 69.

4.8. Littler, T.S., The Physics of the Ear, Pergamon Press, 1965, p. 103.

5. FURTHER EXPERIMENTAL RESULTS

5.1 Wave Speed Study

In order to measure wave speeds in the targets, thereby evaluating relative stiffness, tests were conducted with impact on the ¼-inch-diameter transducer. This was located at approximately the geometric center of the panel. The 1/8-in-diameter transducer, acting as an accelerometer, was located 2.0 inches distant. For the composite targets, the accelerometer was oriented so as to measure wave velocity in the x and y directions (defined by Figure 3.2) as well as in the direction rotated 45° from the panel edges. Figure 5.1 shows the results of these tests for the fiberglass-epoxy panel B2, which exhibited the most extreme anisotropy of any of the materials studied. For all the panels the wave forms were similar. A wave speed was (arbitrarily) taken to be associated with the indicated points in the records. This speed should approximate that of the dominant flexural wave. Wave speeds, c, as defined in this manner are tabulated in Table 5.1.

Table 5.1 Wave Speeds

	c_x(in/s)	c_y(in/s)	c_{45^o}(in/s)
Bonded Aluminum, A3	70,175	-	-
Fiberglass-Epoxy, B2	44,454	31,496	34,482
Graphite-Epoxy, C2	54,054	48,139	-

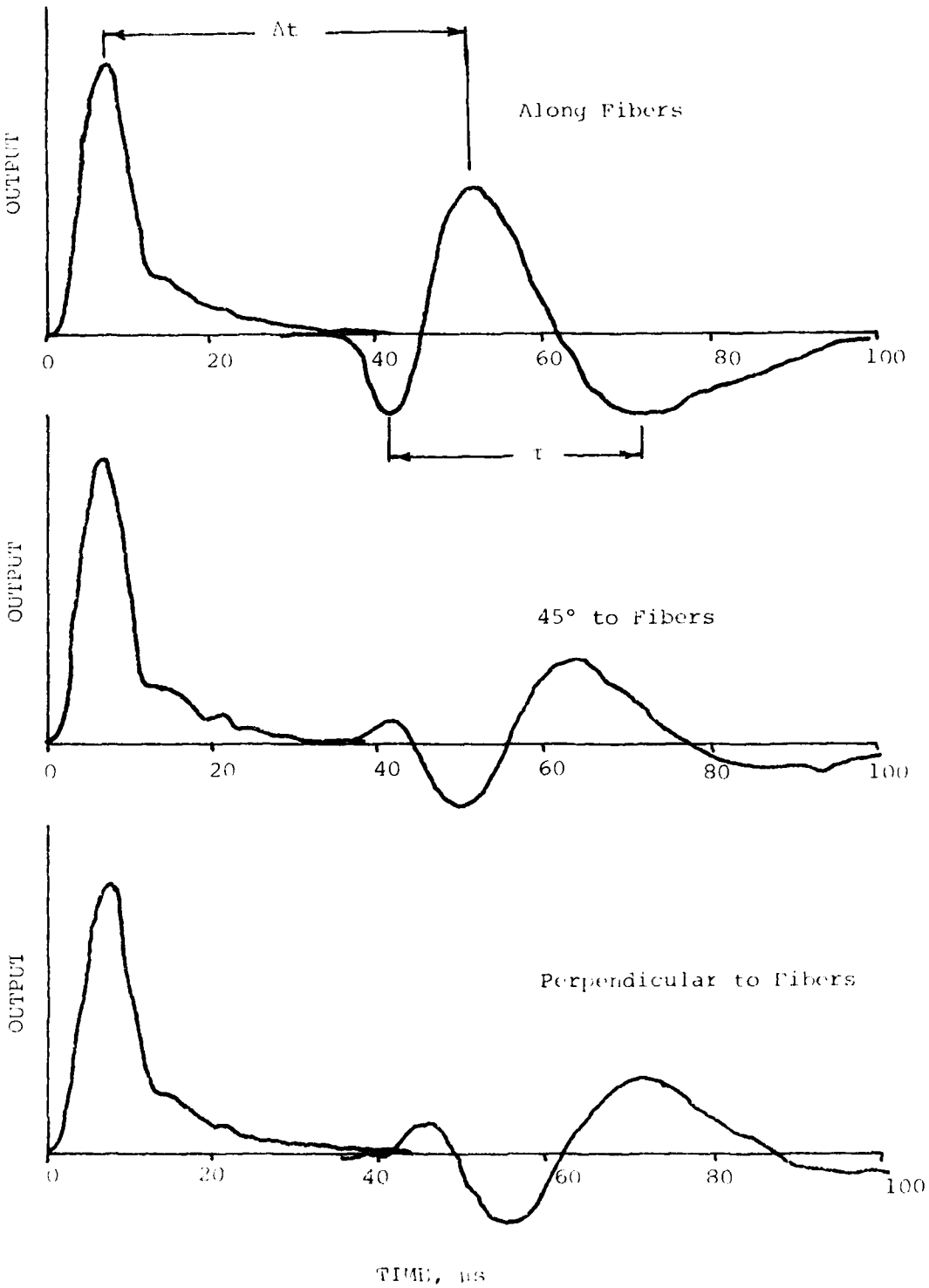

Figure 5.1. Transducer outputs for wave speed experiment on Target B2 (Fiberglass-Epoxy).

5.2 Separated Flaw

The flaws in target A3 were unique in that they consisted of not simply a debonded plane in the material but an actual void. A test sequence along the smaller flaw here produced peak experimental records typified by Figure 5.2. Peak amplitudes for this sequence are plotted in Figure 5.3 for two lines parallel to the plate edge. The ringing portion of these records exhibit a stronger contrast between on- and off- debond records than is the case for the "tight" flaws otherwise tested. This is attributed to the plate halves being sufficiently separated (about 0.009-inches) so that they never come in contact with each other in the debonded region.

5.3 Effect of Flaw Depth on Response

For the composite targets the flaw could be locatd at other depths than mid-thickness. In target B4 the flaw was placed at one-quarter of the depth to permit examination of the effect of flaw depth. By inverting this plate, a flaw depth of three-quarters of the thickness was examined. The results of these tests are shown in Figure 5.4. Flaws are found to be much more apparent when located nearer to the target surface.

5.4 Additional Tests on Fiberglass-epoxy Plates

Additional tests on the series B plates were conducted in order to provide data comparable to that for the A and C series targets. For the ¼-inch-diameter transducer, outputs are shown in Figure 5.5

and 5.6 for the ½-inch-radius and 2-inch radius debonds, respectively. Corresponding plots of peak amplitude versus position are presented in Figures 5.7 and 5.8.

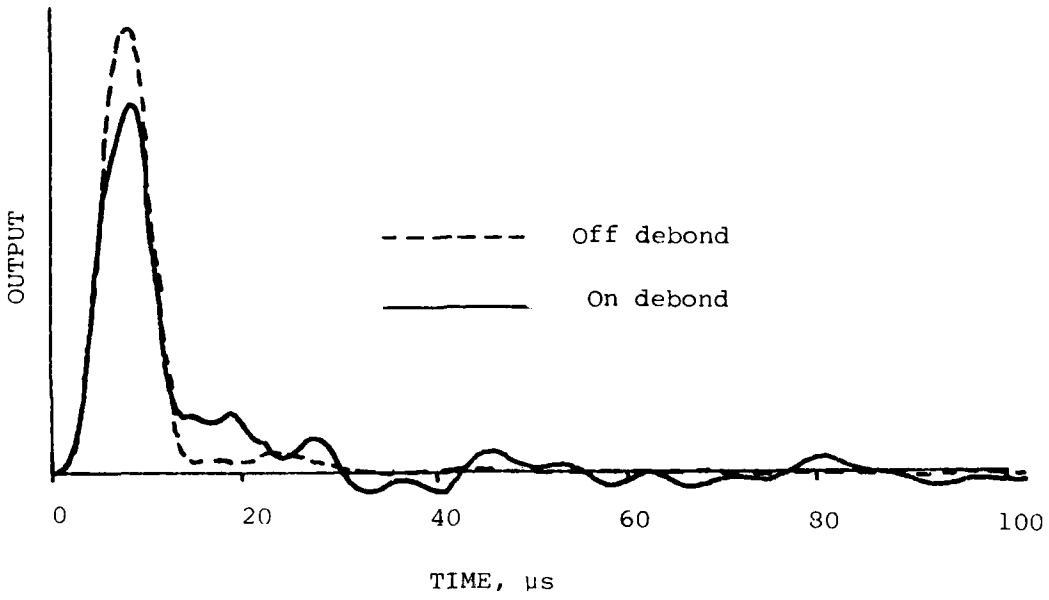

Figure 5.2. Representative transducer outputs for Target A3 (Bonded Aluminum) for loading by the 1/8-inch striker.

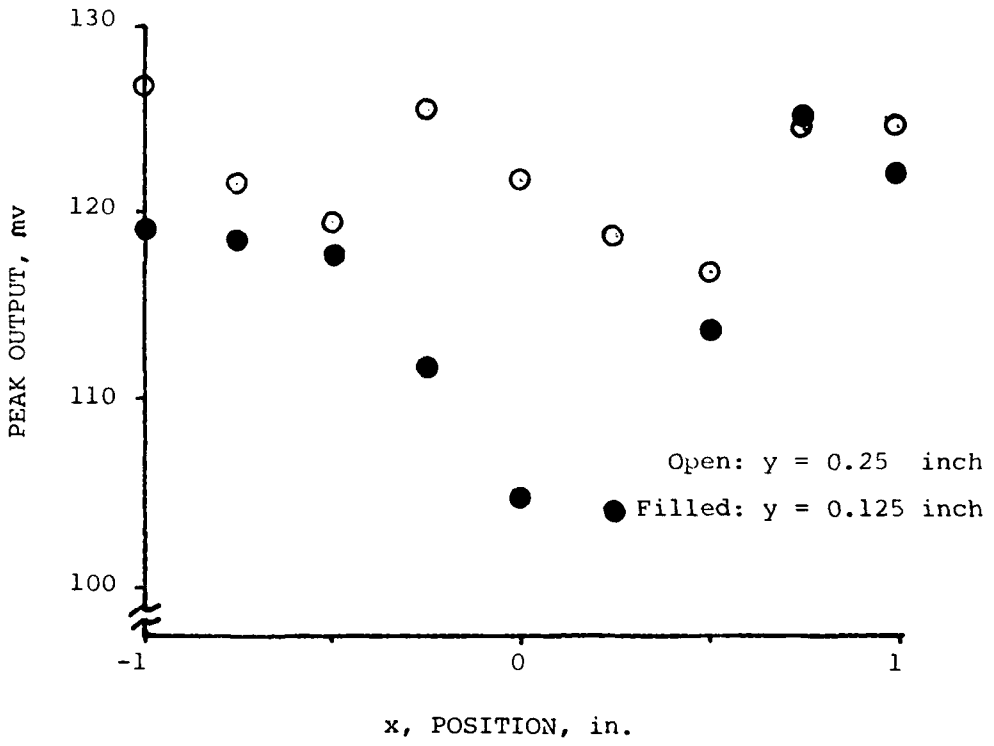

Figure 5.3. Peak transducer outputs vs. position, Target A3 (bonded aluminum).

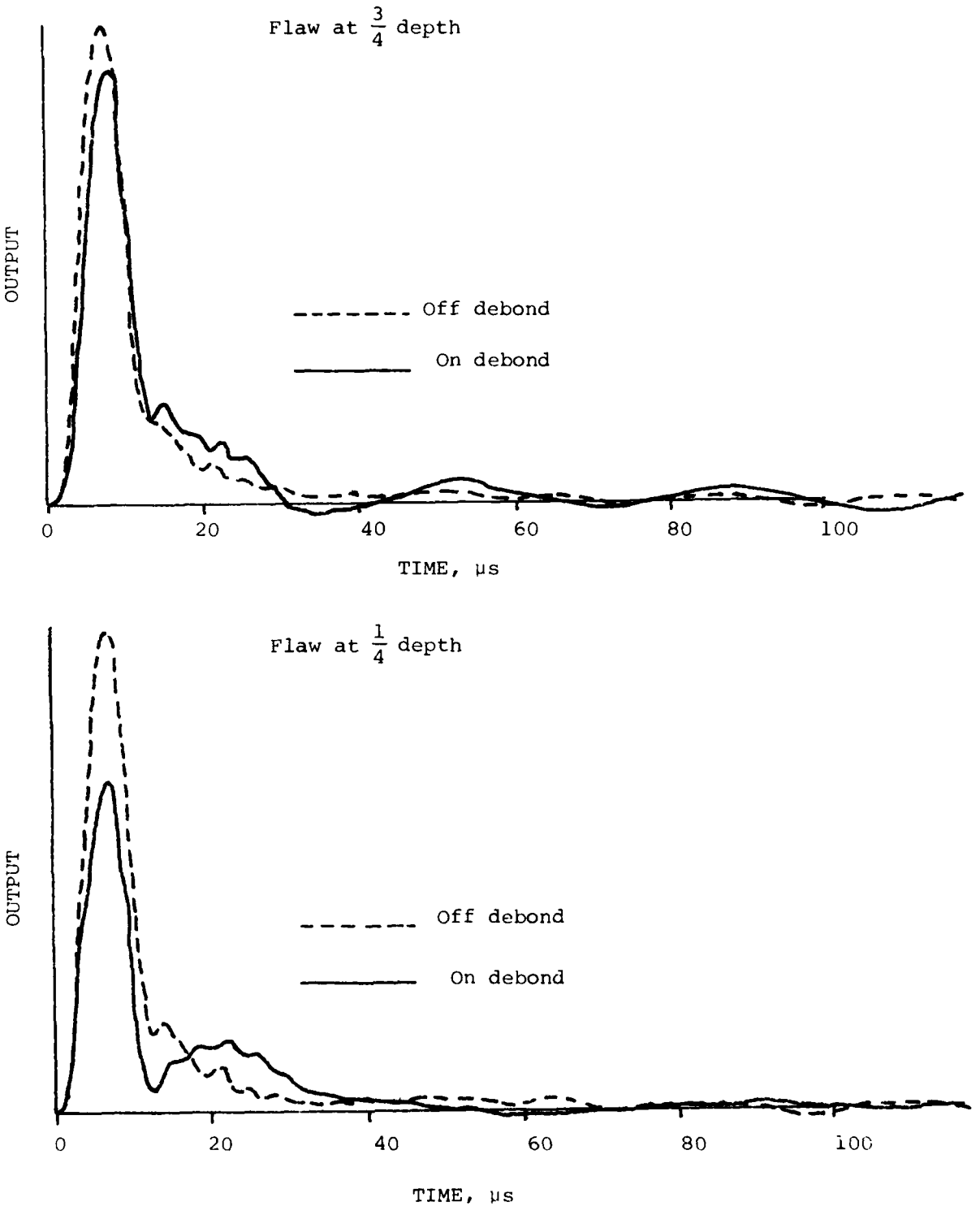

Figure 5.4. The effect of flaw depth in Target B4 (Fiberglass-epoxy).

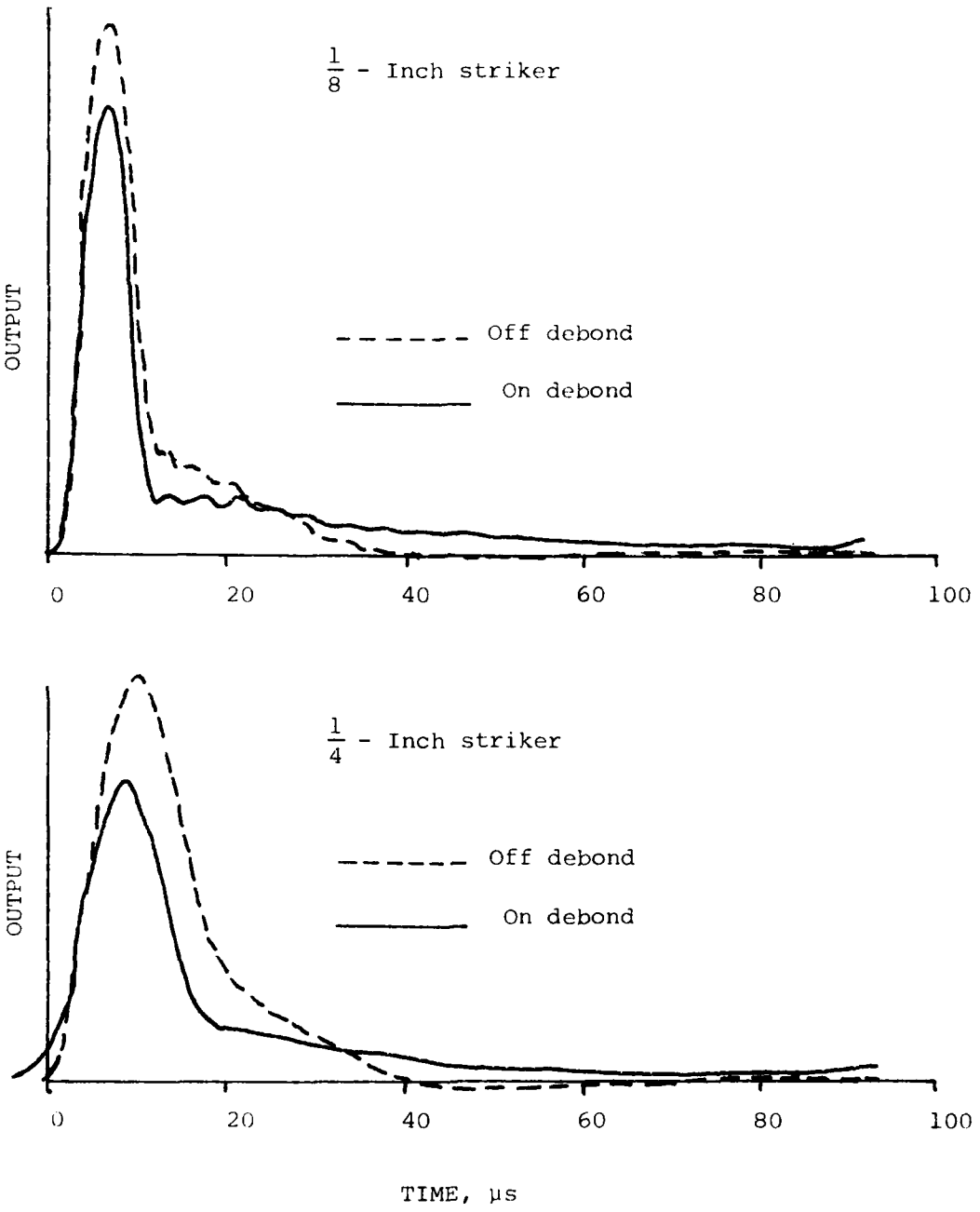

Figure 5.5 Representative transducer outputs for Target B3, 1/2-inch-radius flaw.

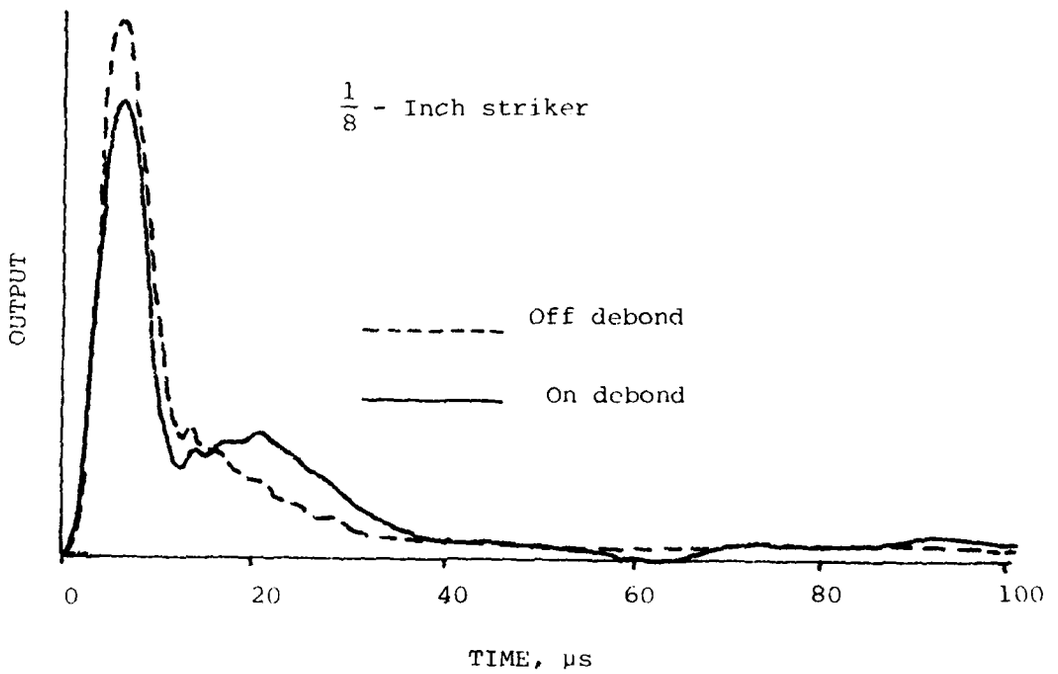

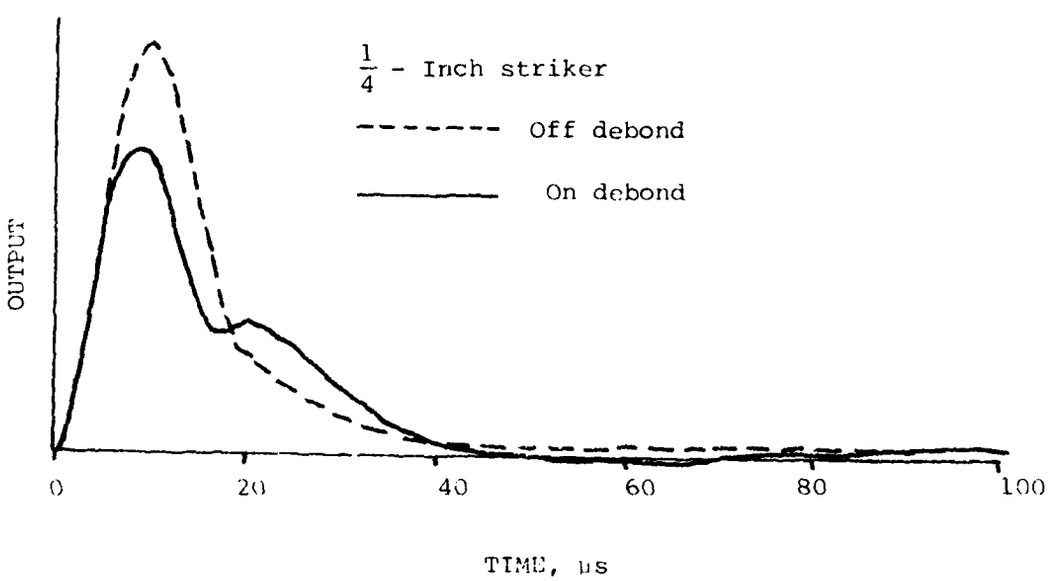

Figure 5.6. Representative transducer outputs for Target B3, 2-inch-radius flaw.

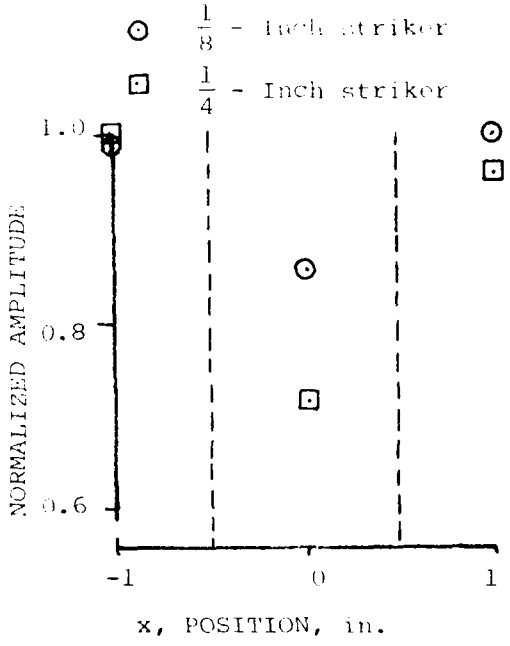

Figure 5.7. Peak transducer outputs vs. position for y = 0.25 inches for Target B3, 1/2-inch-radius flaw.

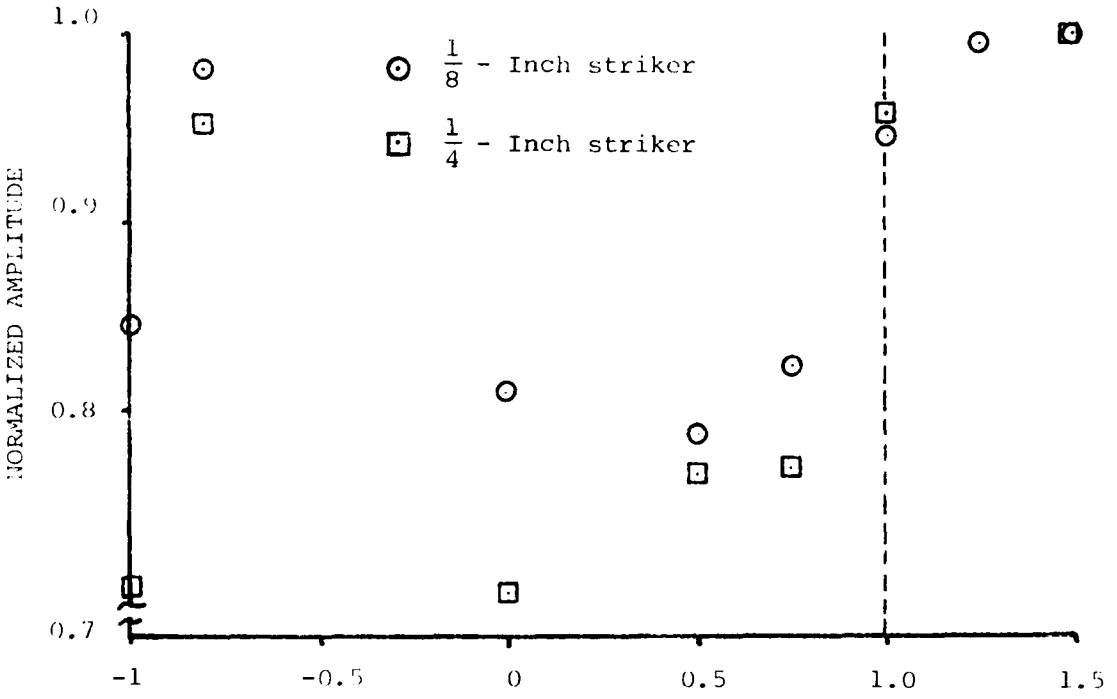

Figure 5.3. Peak transducer outputs vs. position for y = 0.25 inches for Target B3, 2-inch-radius flaw.

6. FINITE ELEMENT MODELLING

6.1 Introduction

Since it is highly nonlinear, the present problem of impact of a sphere on a flawed plate is almost impossible to solve exactly. In searching for an approximate solution, it is natural to resort to the finite element approach. Several attempts have been made to obtain generally applicable techniques for solving contact-impact problems with the finite element method[6.1-6.3]. One approach is to formulate such contact problems from variational inequalities [6.4-6.5]. From the numerical point of view, Francavilla and Zienkiewicz[6.6] proposed a rather simple technique for the numerical computation of frictionless contact problems. Based on this technique, Sachdeva, and Ramakrichnan made an extension to the case with friction[6.7]. The method used to solve the problem here is based on concepts from these previous papers. The difference is that now the problem is a three-dimensional dynamic problem with two contact areas, one between the sphere and the plate and the other at the flaw.

6.2 Method of Analysis

Consider the problem of a general elastic body having a crack as shown in Figure 6.1. The upper surface A and lower surface B can be brought into contact by prescribed external loading. The boundary points along surfaces A and B are close enough to have common normal and tangential directions. At each of these points, let the vector of contact forces be P_i^A for surface A and P_i^B for surface B.

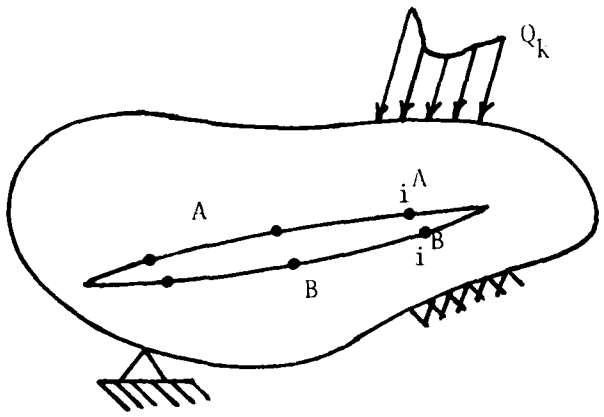

Figure 6.1 Cracked elastic body.

Both of these vectors have three components, one normal and two tangential. Based on the reciprocal formulation[6.5], this nonlinear problem can be decomposed into two linear problems, i.e. the final displacements are superimposed from the displacements due to external loading only and the displacements calculated from the contact forces only. The compatibility condition has to be satisfied during superposition. Now, the displacement of point i^A due to external loading without contact forces will be

$$\delta_i^A = \sum_{k=1}^{m} C_{ik} Q_k \,, \tag{6.1}$$

where m is the number of loading points. The displacement due to the contact forces only is

$$\bar{\delta}_i^A = \sum_{j=1}^{n} \bar{C}_{ij} P_j^A \quad , \tag{6.2}$$

where n is the number of contact points. The total displacment of point i^A is then

$$\Delta_1^A = \delta_i^A + \bar{\delta}_i^A = \sum_{k=1}^{m} C_{ik} Q_k + \sum_{j=1}^{n} \bar{C}_{ij} P_j^A \tag{6.3}$$

where C_{ik} and $\bar{C}_{ij}$ are condensed flexibility matrices. Similiarly,

$$\Delta_i^B = \delta_i^B + \bar{\delta}_i^B = \sum_{k=1}^{m} D_{ik} Q_k + \sum_{j=1}^{n} \bar{D}_{ij} P_j^B \tag{6.4}$$

where D_{ik}, D_{ij} are again condensed flexibility matrices. Up to now, the contact forces P_j are all unknowns. What is needed is the condition of compatibility or impenetrability.

Let the initial separation of surface A and B be Δ_i. The compatibility condition then gives the equations

$$\Delta_i^A = \Delta_i^B + \Delta_i^o \tag{6.5}$$

Substituting for Δ_i^A and Δ_i^B and reformulating the equation gives

$$\phi_i = \sum_{j=1}^{n} E_{ij} P_j \quad ,$$

where (6.6)

$$\phi_i = \sum_{k=1}^{m} C_{ik} Q_k - \sum_{k=1}^{m} D_{ik} Q_k - \Delta_i^o$$

is the penetration of point i and E_{ij}, as shown in Figure 6.2, is the flexibility matrix corresponding to relative displacement, i.e the relative displacement of points i^A and i^B induced by unit contact forces applied both at i^A and i^B. From Equation 6.6, the contact forces can be solved for iteriatively. If the actual contact area is known previously, the problem is reduced to a linear one.

When points slip relative to each other along the contact surface, the compatibility Equation 6.5 will not be valid for the

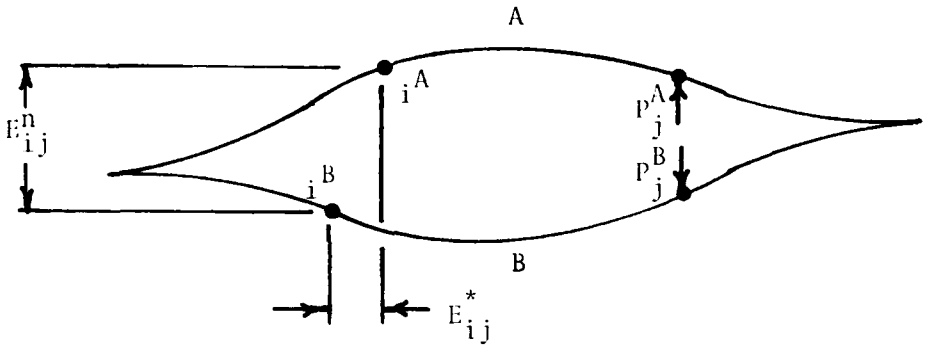

Figure 6.2 Defining displacements at crack surface.

tangential direction. Hence, the Equations 6.5 have to be replaced by the equation

$$P_i^{(t)} = \mu P_i^{(n)} \tag{6.7}$$

along the nodes where the sliding occurs.

In general, the area of contact and the nodes where sliding occurs are not known in advance. Iteration is necessary to check both the contact nodes and the sliding nodes.

When sliding does occur at a node, the tangential component of the contact force corresponding to this node is proportional to its normal component. This case is identical to the displacements along a skew boundary, as shown in Figure 6.3.

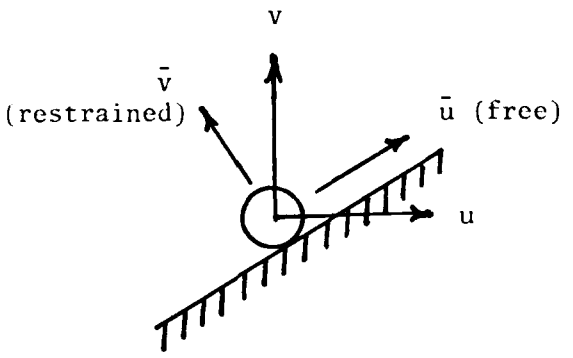

Figure 6.3 Displacement decomposition

The displacement v is proportional to u. To calculate the displacment a transformation is needed[6.8]. This also happens in sliding and a transformation of coordinate along the principal shear direction and normal direction is necessary. It is assumed that the magnitude of sliding is small compared to mesh size.

The procedures of this method are summarized as follows:

1. Solve for the penetration due to external loading.
2. Form the flexibility matrix of relative displacement.

3. Calculate the contact forces including normal and tangential components.
4. Delete all the nodes where contact forces are tension from the possible contact area.
5. Check the ratio of tangential component to the normal component of nodal force at all the nodes in contact.
6. Transform the nodal forces according to the process applied to skew boundary conditions if sliding does occur.
7. Repeat step 3 to 6 until all the normal forces in the contact zone are compression only and the ratio of tangential component to normal component for all the nodes in contact is equal to or less than friction coefficient.

6.3 Finite Element Modelling

The conventional finite element is used in this problem. Since there is a flaw in the plate, 2-D plate elements cannot be used. For a linear shape function, 2x2x2 Gauss integration points are sufficient to give a correct integration[6.10]. To avoid spurious modes of displacement in bonding type elements, a reduced integration technique is necessary[6.9,6.11]. Among several choices of reduced integration, it has been found by comparing the trace of element stiffness matrix, that 2 points of integration in normal components and 1 point in shear components is the best[6.10]. Three dimensional finite element modelling is always time consuming. To save computer time and space, skyline storage is used in every

stiffness and flexibility matrix, and Gauss elimination is used in equation solving.

6.4 References

6.1 Chan, S.H. and I.S. Tuba, "A Finite Element Method for Contact Problems of Solid Bodies", Int. J. Mech. Sci., 13, 615-639 (1971).

6.2 Conry, T.F. and A. Seireg, "A Mathematical Programming Method for Design of Elastic Bodies in Contact", J. Appl. Mech., ASME, 2, 387-392 (1971).

6.3 Hughes, T.J.R., et al, "A Finite Method for a Class of Contact Impact Problems", Comp. Math. in Appl. Mech. and Engrg., 8, 249-276 (1976).

6.4 Duvant, G., and J.L. Lions, Inequalities in Mechanics and Physics", Dunod, Paris (1972).

6.5 Kikuchi, N., "A Class of Signorini's Problems by Reciprocal Variational Inequalities", in Computational Techniques for Interface Problems, K.C. Park and D.K. Gartling (eds.), AMD - Vol. 30, American Society of Mechanical Engineers, 1978.

6.6 Froncavilla, A. and O.C. Zienkiewicz, "A Note on Numerical Computation of Elastic Contact Problem, Int. J. Num. Math. Engrg. Vol. 9, 913-924 (1975).

6.7 Sachdeva, T.D. and C.V. Ramakrishnon, "A Finite Element Solution for the Two-dimensional Elastic Contact Problems with Friction", Int. J. Num. Math. Engrg., Vol. 17, 1257-1271 (1981).

6.8 Bath, K.J. and E.L. Wilson, "Numerical Methods in Finite Element Analysis", Prentice-Hall, Inc., NJ (1976).

6.9 Zienkiewicz, O.C., The Finite Element Method, McGraw-Hill Book Co. (U.K.), (1977)

6.10 Clough, R.W., "Comparison of Three Dimensional Finite Elements", Proceeding of the Symposium on Application of Finite Element Methods in Civil Engineering, ASCE, Nashville, TN, Nov. (1969)

6.11 Zienkiewicz, O.C., R.L. Taylor, and J.M. Too, "Reduced Integration Technique in General Analysis of Plate and Shell", Int. J. Num. Math. Engrg., Vol. 3, 275-290 (1971).

APPENDIX A: PUBLICATIONS UNDER THIS CONTRACT

1. Kenner, V.H., Staab, G.H. and Jing, H.-S, "The Application of a Miniature Force Transducer to the Detection of Edge Flaws in Laminated Plates," Deelopments in Mechanics, v. 12, pp 279-283, May 1983.

2. Kenner, V.H., Staab, G.H. and Jing, H.-S., " A Study of Flaw Identification in Adhesive Bonds using a Technique of Impact Modification," Experimental Mechanics, v. 24, p. 243-247, Sept. 1984.

3. Kenner, V.H., Staab, G.H. and Jing, H.-S., "Quantification of the 'Tapping' Technique for the Detection of Edge Defects in Laminated Plates," In press, American Society for Testing and Materials.

4. Jing, H.-S., Ph.D. Dissertation, Ohio State University, In Preparation.

*U.S.Government Printing Office: 1985 - 559-065/20780

END

FILMED

7-85

DTIC